Published in final edited form as:

Cell Rep. 2021 August 31; 36(9): 109644. doi:10.1016/j.celrep.2021.109644.

Coordination among multiple receptor tyrosine kinase signals controls *Drosophila* developmental timing and body size

Xueyang Pan[1,2], **Michael B. O'Connor**[1,3,*]

[1]Department of Genetics, Cell Biology and Development and the Developmental Biology Center, University of Minnesota, Minneapolis, MN 55455, USA

[2]Present address: Department of Molecular and Human Genetics, Baylor College of Medicine, Houston, TX 77030, USA

[3]Lead contact

SUMMARY

In holometabolous insects, metamorphic timing and body size are controlled by a neuroendocrine axis composed of the ecdysone-producing prothoracic gland (PG) and its presynaptic neurons (PGNs) producing PTTH. Although PTTH/Torso signaling is considered the primary mediator of metamorphic timing, recent studies indicate that other unidentified PGN-derived factors also affect timing. Here, we demonstrate that the receptor tyrosine kinases anaplastic lymphoma kinase (Alk) and PDGF and VEGF receptor-related (Pvr), function in coordination with PTTH/Torso signaling to regulate pupariation timing and body size. Both Alk and Pvr trigger Ras/Erk signaling in the PG to upregulate expression of ecdysone biosynthetic enzymes, while Alk also suppresses autophagy by activating phosphatidylinositol 3-kinase (PI3K)/Akt. The Alk ligand Jelly belly (Jeb) is produced by the PGNs and serves as a second PGN-derived tropic factor, while Pvr activation mainly relies on autocrine signaling by PG-derived Pvf2 and Pvf3. These findings illustrate that a combination of juxtacrine and autocrine signaling regulates metamorphic timing, the defining event of holometabolous development.

Graphical abstract

*Correspondence: moconnor@umn.edu.

AUTHOR CONTRIBUTIONS

Conceptualization, M.B.O. and X.P.; methodology, M.B.O. and X.P.; investigation, X.P. and M.B.O.; writing – original draft, X.P.; writing – review & editing, M.B.O. and X.P.; funding acquisition, M.B.O.; supervision, M.B.O.

SUPPLEMENTAL INFORMATION

Supplemental information can be found online at https://doi.org/10.1016/j.celrep.2021.109644.

DECLARATION OF INTERESTS

The authors declare no competing interests.

INCLUSION AND DIVERSITY

While citing references scientifically relevant for this work, we also actively worked to promote gender balance in our reference list.

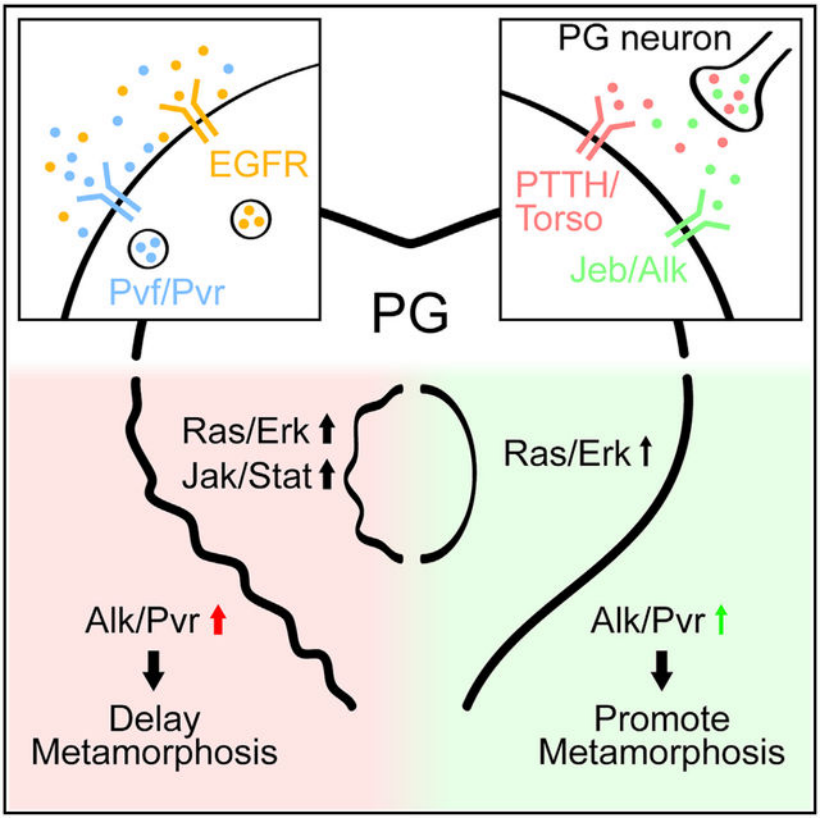

In brief

Pan and O'Connor identify Jeb/Alk and Pvf/Pvr as additional signaling pathways that control developmental timing and body size in *Drosophila*. Jeb/Alk signaling occurs in a juxtracrine fashion between the prothoracic gland (PG) neurons and the PG to control ecdysone production, while Pvf/Pvr signals via autocrine activity within the PG itself.

INTRODUCTION

Body size is one of the most important traits of a multicellular organism. In species whose growth is determinate, the body growth of an individual is largely completed when it matures into an adult (Callier and Nijhout, 2013). A good example of determinate growth is found among holometabolous insects, such as the fruit fly *Drosophila melanogaster*. During development, the size of a *Drosophila* larva increases 100-fold during its three molts, but it does not change after metamorphosis, the developmental stage that transitions the juvenile larval form into the sexually mature adult fly. Therefore, the control of metamorphic timing is a key factor that regulates final body size.

In the past decades, numerous studies in *Drosophila* and other holometabolous insect species have demonstrated that the onset of metamorphosis is regulated through a neuroendocrine signaling axis composed of two central information processing nodes: the prothoracic gland (PG), which produces the metamorphosis inducing steroid hormone ecdysone (E), and a bilateral pair of brain neurons, the PG neurons (PGNs), that innervate the PG and release

the neuropeptide PTTH that stimulates E production (McBrayer et al., 2007; Yamanaka et al., 2013a, 2015). After release into the hemolymph, E is taken up by peripheral larval tissues through a specific importer (EcI) and then converted into its active form, 20-hydroxyecdysone (20E), by the enzyme Shade (Okamoto et al., 2018; Petryk et al., 2003) Subsequently, 20E stimulates metamorphosis via activation of the EcR/Usp receptor complex and stimulation of tissue-specific downstream transcriptional cascades (Hill et al., 2013).

In this scheme, PTTH functions as a trophic hormone to stimulate PG growth and E synthesis (Shimell et al., 2018; Smith and Rybczynski, 2012). In PG cells, PTTH binds to Torso, a receptor tyrosine kinase (RTK) family member, and stimulates the E biosynthetic pathway via Ras/Erk signaling (Rewitz et al., 2009). As the two central nodes on the neuroendocrine axis, both the PG and the PGNs receive additional diverse internal and external signals to modulate their output appropriately. For instance, the PG cells respond to insulin signals reflecting the general nutritional state (Colombani et al., 2005; Mirth et al., 2005). In addition, systemic bone morphogenetic protein (BMP) signals help coordinate metamorphosis with appropriate imaginal disc growth (Setiawan et al., 2018). The PGNs in turn, receive presynaptic inputs from various upstream neurons that regulate circadian and pupation behaviors (Deveci et al., 2019; Imura et al., 2020; McBrayer et al., 2007). They also respond to tissue damage signals to delay maturation onset until the damage is resolved (Colombani et al., 2012, 2015; Garelli et al., 2012, 2015; Vallejo et al., 2015).

Although it is widely accepted that PTTH is the key neuropeptide that triggers developmental maturation in holometabolous insects (Deveci et al., 2019; McBrayer et al., 2007; Shimell et al., 2018; Smith and Rybczynski, 2012), several studies indicate that additional timing signals are also likely. The first suggestion that PTTH is not the sole prothoracicotropic signal came from PGN ablation studies in *Drosophila* where it was found that up to 50% of animals with no PGNs still undergo metamorphosis, but after a prolonged ~5-day developmental delay (Ghosh et al., 2010; McBrayer et al., 2007). Subsequently, it was found that genetic null mutations in the *Drosophila* PTTH gene only produced a 1-day developmental delay and had little effect on viability (Shimell et al., 2018). In this case electrical stimulation of the mutant PGNs restored proper timing while inactivation produced a more substantial 2-day delay (Shimell et al., 2018). *Ptth* null mutants have also been generated in *Bombyx mori*, and while most animals arrest development at late larval stages, a fraction still escape and produce adults (Uchibori-Asano et al., 2017). Taken together, these studies strongly indicated that the PGNs produce additional timing signals besides PTTH.

RTK family receptors have been speculated to mediate the additional PGN signal, since blocking the Ras/Erk pathway in the PG causes strong developmental defects, phenocopying the PGN ablation model rather than the *ptth* mutant (Cruz et al., 2020; Rewitz et al., 2009). Epidermal growth factor receptor (Egfr) has recently been implicated in regulating PG tissue growth, E synthesis, and secretion. However, the Egfr pathway is activated by autocrine signals from the PG, which does not involve the activity of PGNs (Cruz et al., 2020). In the present study, we identify two additional RTK family receptors, anaplastic lymphoma kinase (Alk) and PDGF and VEGF receptor-related (Pvr), which play important roles in the PG

controlling metamorphic timing. Interestingly, the Alk ligand Jelly belly (Jeb) and Pvr ligand Pvf3 are both expressed in the PGNs, verifying that the prothoracicotropic function of PGNs is mediated by multiple signaling molecules, while Pvf2 and Pvf3 are also expressed in the PG itself and likely provide additional autocrine signals that also contribute to metamorphic timing control.

RESULTS

Targeted screening of *Drosophila* RTKs for factors controlling developmental timing

Based on the speculation that RTKs could mediate the trophic signals from PGNs to the PG, we performed a targeted RNAi screening using the PG-specific *phm-Gal4* driver to identify RTKs in the PG that regulate the timing of pupariation. Since the knockdown efficiency of the RNAi construct varies, we carried out screening using RNAi lines from the Transgenic RNAi Project (TRiP) and compared the results with recently published genome-wide screening using RNAi lines from the Vienna *Drosophila* Resource Center (VDRC) (Danielsen et al., 2016). Insulin receptor (InR) and Torso, whose functions in the PG have already been readily documented (Colombani et al., 2005; Mirth et al., 2005; Rewitz et al., 2009), were identified in both screens. In addition, we found Alk and Egfr as hits in our TRiP screen while Pvr was a potential hit in the previous genome-wide screen (Table S1). Since the role of Egfr in the PG has been recently documented (Cruz et al., 2020), we focused our efforts on elucidating the roles of Alk and Pvr in the regulation of metamorphic timing and body size.

Alk and Pvr are required for normal metamorphic timing and body size control

Following the initial screen, we first sought to verify the developmental timing phenotype of Alk and Pvr suppression larvae using multiple RNAi constructs as well as dominant-negative receptors. In line with the screening result, knocking down *Alk* in the PG using two different RNAi constructs caused developmental delay. Furthermore, overexpressing dominant-negative Alk resulted in developmental arrest in the L3 stage (Figures 1A and S1A). Similarly, the developmental delay phenotype of Pvr suppression larvae was produced by two independent *Pvr* RNAi constructs, and a third produced developmental arrest. In addition, expression of a dominant-negative Pvr in the PG also produced developmental delay (Figures 1A and S1B).

Using immunofluorescence staining, we examined the expression of *Alk* and *Pvr* in the PG and tested knockdown efficiency of the RNAi lines used above. In control larvae, strong expression of *Alk* and *Pvr* was observed in the PG of late L3 stage larvae, reflected by the distinct fluorescence signals on the PG cell membrane (Figure 1B). Interestingly, the expression of both receptors was remarkably weaker in the early L3 stage (Figure 1B), indicating that the signal outputs from these receptors may be stronger in the late L3 stage when larvae approach the onset of metamorphosis. When expressing *Alk* and *Pvr* RNAi (*UAS-Alk*$^{RNAi\ \#1}$ and *UAS-Pvr*$^{RNAi\ \#2}$) (Figures S1A and S1B), we found that the expression of both receptors in the PG was effectively depleted in the late L3 stage (Figure 1B). Since these RNAi constructs induce efficient gene knockdown, we used them in our following studies. When knocking down either *Alk* or *Pvr* alone, we

observed minor developmental delay. However, simultaneous knockdown of both receptors by *phm>Alk^{RNAi},Pvr^{RNAi}* leads to a more prolonged developmental delay (Figure 1A). Thus, we conclude that both Alk and Pvr act in the PG to regulate metamorphic timing, perhaps in an additive manner. As for the developmental arrest phenotype observed in other crosses (*phm>Alk^{DN}* and *phm>Pvr$^{RNAi\ \#3}$*) (Figures S1A and S1B), we speculate that they may result from unknown detrimental effects from the transgenes or the genetic background of these lines.

In addition to timing, we measured the pupal size of Alk and Pvr suppression animals. The sizes of *phm>Alk^{RNAi}* and *phm>Pvr^{RNAi}* pupae are larger than those of the *phm>w1118* controls, while the *phm>Alk^{RNAi},Pvr^{RNAi}* animals formed pupae of even larger sizes (Figure 1C). We conclude that both Alk and Pvr are required in the PG for normal developmental timing and body size control.

Loss of Alk and Pvr causes stronger developmental defects in *ptth* mutants

The mild developmental delay phenotype of Alk and Pvr suppression animals is comparable to that of *ptth* mutants (Shimell et al., 2018). Since Alk, Pvr, and Torso are all RTKs, we propose that the Alk and Pvr pathways may function additively or synergistically with the PTTH/Torso pathway to control developmental timing. To test this possibility, we knocked down Alk and Pvr in the PG of *ptth* mutants and examined whether the timing of pupariation was further prolonged. Consistent with our conjecture, both *ptth;phm>Alk^{RNAi}* and *ptth;phm>Pvr^{RNAi}* larvae took longer to pupariate than the *phm-Gal4* and no driver (ND) controls and 30% of *ptth;phm>Alk^{RNAi}* larvae failed to pupariate (Figure 1D). Moreover, longer developmental delay and higher rates of developmental arrest at the L3 stage were observed in *ptth;phm>Alk^{RNAi},Pvr^{RNAi}* larvae in which all three RTK pathways were suppressed (Figure 1D). In parallel to the developmental timing change, the pupal size of double or triple RTK suppression animals were also larger than controls (Figure 1E). These data demonstrate that the Alk and Pvr work in association with PTTH/Torso and suggest that the receptors may share the same downstream signaling pathway to regulate developmental timing.

Alk and Pvr facilitate E synthesis and Halloween gene expression by activating the Ras/Erk pathway

It is well established that PTTH/Torso signaling facilitates pupariation activity by stimulating E synthesis in the PG via Ras/Erk pathway (Rewitz et al., 2009). To determine whether Alk and Pvr function via the same mechanism, we first examined the E level in Alk and Pvr suppression larvae. In mid-L3 stage, we did not observe a significant difference in the E level among *phm>w1118*, *phm>Alk^{RNAi}*, *phm>Pvr^{RNAi}*, and *phm>Alk^{RNAi},Pvr^{RNAi}* animals. However, at the time point when *phm>w1118* larvae are at the wandering stage the receptor suppression larvae produce a markedly lower level of E than *phm>w1118* controls (Figure 2A), suggesting that the E synthesis is compromised when Alk and/or Pvr is suppressed in the PG.

Ecdysone is synthesized from cholesterol through the action of E biosynthetic enzymes encoded by the Halloween genes (Niwa and Niwa, 2014). To determine how Alk and Pvr

affects E synthesis in the PG, we assessed Halloween gene expression in *phm>w1118* larvae at the wandering stage and receptor suppression larvae of equivalent age. In *phm>Alk^{RNAi}*, *phm>Pvr^{RNAi}*, and *phm>Alk^{RNAi},Pvr^{RNAi}* larvae, the expression levels of five out of seven Halloween genes (*nvd*, *cyp6t3*, *phm*, *dib*, *sad*) were significantly lower than those in the *phm>w1118* control (Figure 2B). In addition, the expression of *sro* was suppressed in *phm>Alk^{RNAi},Pvr^{RNAi}* double suppression larvae, although in *phm>Alk^{RNAi}* or *phm>Pvr^{RNAi}* larvae no significant change was observed compared with *phm>w1118* (Figure 2B). These results show that Alk and Pvr signaling regulates E biosynthesis by affecting Halloween gene expression.

Previous work has established that both Alk (Englund et al., 2003; Gouzi et al., 2011; Lorén et al., 2001) and Pvr (Learte et al., 2008; Sansone et al., 2015) are able to activate the Ras/Erk pathway in certain *Drosophila* embryonic and post-embryonic tissues. Thus, we tested whether the two pathways activate Ras/Erk signaling in the PG. Since other RTKs, including Torso and Egfr, also activate Ras/Erk signaling in the PG (Cruz et al., 2020; Rewitz et al., 2009), we speculated that partial suppression of Ras/Erk signaling, if it occurs, could be difficult to detect. To circumvent this possible obstacle, we asked whether we could detect a change in Ras/Erk signaling in Alk and Pvr activation larvae. Unexpectedly, overexpressing *Alk* or *Pvr* using the *phm-Gal4* driver caused developmental arrest at an early stage (see below), so we employed *spok-Gal4*, a weaker PG driver for receptor activation/overexpression conditions. To detect the activation level of Ras/Erk signaling, we examined PG immunofluorescence using an antibody that specifically recognizes phosphorylated (phospho-)Erk (Cruz et al., 2020; Ohhara et al., 2015). In *spok>w1118* larvae, the Ras/Erk signaling in the PG appears weak in the early L3 stage and is then activated in the middle L3 stage, as indicated by the enhanced overall immunofluorescence signal strength as well as the partial nuclear localization of the signal (Figure 2C). When constitutively activated (CA) Alk or wild-type Pvr was expressed in the PG by *spok>Alk^{CA}* and *spok>Pvr*, respectively, Ras/Erk was strongly activated in the early L3 stage (Figure 2C), indicating that both Alk and Pvr pathways activate Ras/Erk signaling in the PG. This result is consistent with at least partial overlap between Alk, Pvr, and Torso signaling through Ras/ERK activation.

Alk regulates autophagy in the PG by activating the PI3K/Akt pathway

In addition to Ras/Erk, PI3K/Akt is another signaling pathway activated by RTKs (Mele and Johnson, 2019). A well-studied RTK that activates PI3K/Akt signaling in the PG is InR, which conveys nutritional signal to the PG and promotes PG growth (Caldwell et al., 2005; Colombani et al., 2005; Mirth et al., 2005). Interestingly, one study indicates that Alk is also able to activate PI3K/Akt signaling and to compensate the loss of the InR pathway in multiple larval tissues (Cheng et al., 2011). Therefore, we tested whether Alk and Pvr activate PI3K/Akt signaling in the PG.

To monitor the activation of PI3K/Akt, we expressed a GFP-tagged PH domain (tGPH), which binds specifically to phosphatidylinositol 3,4,5-trisphosphate (PIP3) produced by activated PI3K on cell membrane. First, we tested whether knocking down either *Alk* or *Pvr* causes suppression of the PI3K/Akt pathway. Neither starvation treatment nor the

knockdown of *Alk* or *Pvr* causes any obvious change in tGPH localization in late L3 stage (24 h after L3 ecdysis [AL3E]) larvae (Figure S2A), perhaps due to the existence of insulin signaling and the slow response of tGPH translocation to the change in PI3K/Akt signaling. To overcome this, we sought to detect activation of PI3K/Akt using early L3 stage (0–4 h AL3E) larvae in which the PI3K/Akt activation level is much weaker than that in the late L3 stage larvae (Ohhara et al., 2015). In the early L3 stage, a comparatively weak level of PI3K/Akt activation was observed in the PGs of *spok>w1118* larvae (Figure 3A). The membrane-localized GFP signal was much stronger in the PGs expressing activated InR, consistent with the known capability of InR to activate PI3K/Akt signaling (Weinkove and Leevers, 2000). A comparable strong membrane GFP signal was observed in $spok>Alk^{CA}$ PG cells (Figure 3A), showing that Alk activation can induce PI3K/Akt signaling in the PG. However, no such signal was identified in *spok>Pvr* PGs (Figure 3A). Since both InR and Alk activate PI3K/Akt signaling, we sought to determine whether Alk can compensate the loss of InR signaling in the PG. Overexpressing either activated InR or Alk caused precocious pupariation (Figure 3B), suggesting similar activities of the two receptors in the PG. Suppressing InR activity by $phm>InR^{DN}$ delayed the timing of pupariation, which is effectively rescued by activated Alk (Figure 3B). These results suggest that Alk activates PI3K/Akt signaling and perhaps functions to supplement the InR pathway in the PG.

Autophagy is a process modulated by PI3K/Akt signaling that has been reported to regulate E biosynthesis by altering cholesterol metabolism in the PG (Pan et al., 2019; Texada et al., 2019). Thus we tested whether Alk suppression affects autophagy induction in the PG. Previously, we have shown that autophagy is strongly induced by starvation in the early, but not the late, L3 stage (Pan et al., 2019). Since Alk is highly expressed in the late L3 stage (Figure 1B), we hypothesized that Alk signaling may be responsible for suppressing autophagy induction during late-stage development. To test this possibility, we analyzed autophagy induction in the PG using *phm>mCherry-Atg8a* in fed and starved late L3 larvae. By measuring both the number and the area of Atg8a-positive puncta, we found that autophagy is significantly induced in $phm>Alk^{RNAi}$ larvae in both the fed and starvation conditions (Figures 3C–3E). Activation of the Alk signal suppressed starvation-induced autophagy in early L3 stage larvae, further confirming the function of Alk on suppressing autophagy (Figures 3F–3H). In contrast, knocking down *Pvr* in the PG did not affect autophagy induction (Figures 3C–3E), in agreement with the finding that Pvr does not induce PI3K/Akt signaling. Taken together, we conclude that Alk, but not Pvr, suppresses the inducibility of PG autophagy induction in late-stage larvae.

Activation of Alk and Pvr pathways affects developmental timing in a dose-dependent manner

Since suppression of Alk and Pvr delays the timing of pupariation, we tested whether activation of the receptors accelerates developmental timing. Alk and Pvr activation by $spok>Alk^{CA}$ and *spok>Pvr* resulted in earlier pupariation and formation of smaller pupae (Figures 4A and 4B), which is consistent with our hypothesis that they contribute to the developmental timing signal. Upon activation of Alk or Pvr in *ptth* mutants, the developmental delay and larger pupal size caused by the loss of *ptth* were reversed by

Alk and Pvr activation (Figures 4C and 4D), showing that activation of Alk and Pvr can compensate for loss of PTTH/Torso signaling.

Curiously, when Pvr signaling is further stimulated through expression of CA Pvr (*spok>Pvr^{CA}*), many larvae failed to pupariate and the rest pupariated no earlier than did the *spok>w1118* controls (Figure 4A). Furthermore, as mentioned above, overexpressing Alk and Pvr using the strong *phm-Gal4* PG driver results in developmental arrest before larvae reach the L3 stage. Based on these observations using different Alk/Pvr activation models, we hypothesized that the effect of Alk and Pvr activation on developmental timing is "dose-dependent." That is, weak/moderate activation of Alk and Pvr causes precocious pupariation, but high-level activation leads to detrimental effects on development. To verify this dose-dependence hypothesis, we employed a *spok^{GeneSwitch}-Gal4* whose Gal4 driver strength is determined by the concentration of RU486 administration (Roman et al., 2001). In *spok^{GeneSwitch}>Alk^{CA}* larvae, a low dose of RU486 feeding (0.1 μg/mL) caused earlier pupariation, while a high dose (5.0 μg/mL) led to a high rate of developmental arrest in the L3 stage (Figure 4E). A mid-level dose (1.0 μg/mL) caused a mixed phenotype of precocious pupariation and developmental arrest (Figure 4E), confirming the bi-phasic, dose-dependent effects of Alk activation on developmental timing. Similar results were observed in *spok^{GeneSwitch}>Pvr^{CA}* larvae, with the only difference being that the mid-level dose RU486 caused a higher rate of developmental arrest (Figure 4F). These data demonstrate that moderate, but not high-level, activation of Alk and Pvr accelerates the timing of pupariation.

To explore the mechanism underlying the detrimental effect caused by receptor overactivation, we initially examined PG morphology in the receptor activation larvae. PG tissue overgrowth was found in all *spok>Alk^{CA}*, *spok>Pvr*, and *spok>Pvr^{CA}* larvae (Figure S3A). However, only the *spok>Pvr* PG exhibited uniform cell and nuclear sizes, which was also observed in *spok>InR^{CA}* PGs (Figure S3A). In both *spok>Alk^{CA}* and *spok>Pvr^{CA}* PGs, cells exhibited extensive heterogeneity and loss of normal tissue organization (Figure S3A), reminiscent of the atypical morphology of cancerous tissues. Based on these observations, we speculate that the atypical growth of the PG is likely even worse in *phm-Gal4*-driven receptor overactivation animals and it produces developmental arrest because of PG cell malfunction or death.

Previous studies have shown that simultaneous activation of Ras/Erk and Jak/Stat signaling induces cancerous-like growth in *Drosophila* larval tissues (Wu et al., 2010). Gain-of-function alleles of *Torso* have also been found to induce activation of the Jak/Stat pathway during embryonic development (Li et al., 2002). Inspired by these observations, we tested whether Jak/Stat signaling is activated by either Alk or Pvr. Using 10xStat92E-GFP, a reporter of Jak/Stat signaling, we observed remarkably strong GFP signal in *spok>Alk^{CA}*, *spok>Pvr*, and *spok>Pvr^{CA}* PGs (Figure S3B), clearly showing that both Alk and Pvr activation can induce Jak/Stat signaling in the PG. Interestingly, *spok>Torso* did not induce strong Jak/Stat activation in the PG, despite the ability of activated alleles to do so in some embryonic tissues (Figure S3B) (Li et al., 2002), perhaps again indicating that dose is an important factor when considering which downstream pathways can be activated by these different RTKs.

We next investigated whether Jak/Stat signaling mediated the developmental defects caused by Alk and Pvr overactivation. We used *phm-Gal4* to induce overactivation of the receptors and suppressed the Jak/Stat pathway by *UAS-Stat92E*^{RNAi}. Since *UAS-Stat92E*^{RNAi} could weaken the driver strength of *phm-Gal4*, we introduced *UAS-mCD8GFP* in the control groups without *UAS-Stat92E*^{RNAi} to dilute *phm-Gal4* strength. Both *phm>mCD8GFP,Alk*^{CA} and *phm>mCD8GFP,Pvr*^{CA} larvae were arrested at various larval stages before pupariation (Figure 4G). Knockdown of *Stat92E* did not significantly affect developmental timing by itself. However, the developmental arrest caused by *phm>mCD8GFP,Alk*^{CA} and *phm>mCD8GFP,Pvr*^{CA} was effectively rescued in *phm>Stat92E*^{RNAi}*,Alk*^{CA} and *phm>Stat92E*^{RNAi}*,Pvr*^{CA} animals, respectively (Figure 4G). These results demonstrate that Jak/Stat signaling induced by Alk and Pvr overactivation mediates the developmental defects in Alk and Pvr overactivation animals. Since Jak/Stat is very weakly induced in *phm>w1118* control animals (Figure S3C), we conclude that Alk and Pvr do not strongly activate Jak/Stat signaling in wild-type animals, but they may do so under certain developmental or environmental conditions.

Ligands that activate Alk and Pvr derive from both PGNs and PG

After confirming the effect of Alk and Pvr on developmental timing and body size control, we sought to determine the source of their ligands that activate the receptors in the PG. Based on our previous observations that ablation of PGNs produces a stronger phenotype than does loss of *ptth* (Shimell et al., 2018), we speculate that some level of ligand may derive from the PGNs. However, autocrinal regulation pathways have also been discovered in the PG (Cruz et al., 2020; Ohhara et al., 2015), indicating that the ligands may also be produced by the PG itself. Therefore, we tested for ligand expression in both PGs and PGNs.

Since Jeb is the only known ligand for Alk (Englund et al., 2003), we first sought to detect *jeb* expression using fluorescence *in situ* hybridization (FISH) and found that *jeb* mRNA is found in the PGNs (Figure S4A). Since the Jeb fluorescence signal in the FISH experiment was weak, we further examined the expression pattern of Jeb by taking advantage of the *Minos* Mediated Integration Cassette (MiMIC) insertion fly line (*jeb*^{MI03124}) (Nagarkar-Jaiswal et al., 2015) and converting it into a Gal4 expression line (*jeb*^{T2A}*-Gal4*) using the recombinase-mediated cassette exchange (RMCE) strategy (Diao et al., 2015; Li-Kroeger et al., 2018). In the *jeb*^{T2A}*>EGFP* larvae, we observed *jeb* expression in numerous larval brain lobe neurons, while no obvious expression was detected in the PG (Figure S4B). By immunostaining using anti-PTTH antibody, we clearly found overlap between the EGFP and the PTTH signals (Figure 5A), showing that *jeb* is expressed in the PGNs.

Unlike Alk, Pvr has three known ligands, Pvf1, Pvf2, and Pvf3. To determine which of the Pvf ligands activate Pvr in the PG, we first tested the viability of null mutants of the three genes. The *Pvf2*^{T2A}*-Gal4* and *Pvf3*^{T2A}*-Gal4* larvae, in which the endogenous *Pvf* gene expression is disrupted by the T2A cassette insertion (Diao et al., 2015), did not survive into the L3 stage. However, a well-characterized null mutant *Pvf1*^{EP1624} (Duchek et al., 2001) pupariated without significant delay (Figure S4C). Therefore, we speculate that Pvf2 and Pvf3, but not Pvf1, may be the ligands that interact with Pvr in the PG. Using the T2A-Gal4 lines generated from *Pvf2*^{MI00770} and *Pvf3*^{MI04168}, we observed *Pvf3* expression in the

PGNs (Figure 5B), while both *Pvf2* and *Pvf3* were expressed in the PG (Figures 5C and 5D). Intriguingly, the expression of *Pvf2* and *Pvf3* in the PG exhibited different temporal patterns. *Pvf2* expression is limited in the early L3 stage but surges in the late L3 stage (Figure 5C), while *Pvf3* expression is high throughout the L3 stage (Figure 5D).

We next tested whether these ligands are required for the effects of Alk and Pvr signaling on pupariation timing control. Using the *NP423-Gal4* driver, which is active in the PGNs, (Yamanaka et al., 2013b), we first knocked down *jeb* or *Pvf3* in the PGNs. Depletion of Jeb in the PGNs using two RNAi constructs caused delayed pupariation and enlarged pupal size (Figures 5E and 5F), showing that the activation of Alk in the PG is, at least partially, mediated from the PGN-derived Jeb signal. However, knockdown of *Pvf3* in the PGNs did not significantly affect pupariation timing (Figures S4D and S4E), indicating that Pvr signaling does not fully depend on the PGN-derived Pvf3. We then sought to test whether PGN-derived Jeb and Pvf3 function in cooperation with PTTH. Knocking down *jeb* using *NP423-Gal4* in *ptth* mutants resulted in prolonged developmental delay (Figure 5G) and larger pupal size (Figure 5H), confirming the contribution of the PGN-derived Jeb signal to the control of developmental timing and body size. However, *jeb* and *Pvf3* double knockdown in *ptth* mutants did not further delay development or affect body size (Figures 5G and 5H), corroborating the minor role of PGN-derived Pvf3 in developmental timing and body size regulation.

Next, we suppressed the expression of *Pvf2* and *Pvf3* in the PG using multiple RNAi constructs. Neither *Pvf2* nor *Pvf3* knockdown caused a significant delay in developmental timing, except for one *Pvf2* RNAi ($phm>Pvf2^{RNAi\ \#3}$), which resulted in a minor timing delay (Figures S4F–S4I). However, when both ligands were simultaneously knocked down in the PG using $phm>Pvf2^{RNAi},Pvf3^{RNAi}$, we observed significant delay of timing and enlarged pupae compared with *phm>w1118* control (Figures 5I and 5J). This result shows that both Pvf2 and Pvf3 likely activate Pvr by an autocrine pathway, although some contribution of PGN-derived Pvf3 cannot be ruled out.

Lastly, we examined whether overexpression of the ligands could phenocopy the receptor activation animals. Neither Jeb/Pvf3 overexpression in the PGNs nor Pvf2/Pvf3 overexpression in the PG induced a significant change in the timing of pupariation (Figure S4J–S4M), showing that the activity of the Alk and Pvr pathways in the PG is not solely controlled by expression of the ligands.

DISCUSSION

Multiple RTK signals coordinate in the PG to regulate developmental timing

In previous studies, three RTKs, that is, Torso (Rewitz et al., 2009), InR (Colombani et al., 2005; Mirth et al., 2005), and Egfr (Cruz et al., 2020), have been demonstrated to be crucial in the PG for the control of pupariation and body size. In this work, we identified two additional RTKs, Alk and Pvr, that are also required for proper timing and body size control. Suppression of either Alk or Pvr compromises E synthesis in the PG (Figure 2A), delays pupariation (Figure 1A), and increases pupal size (Figure 1C), while moderate activation of Alk or Pvr accelerates development (Figure 4A). The biological functions of

Alk/Pvr in the neuroendocrine pathway are similar to those of the other RTKs (Colombani et al., 2005; Cruz et al., 2020; Mirth et al., 2005; Rewitz et al., 2009), indicating likely signal coordination among the receptors. Downstream signaling from Torso (Rewitz et al., 2009), Egfr (Cruz et al., 2020), Alk, and Pvr (Figure 2C) all involve activation of Ras/Erk signaling, while InR (Mirth et al., 2005) and Alk (Figure 3A) can also stimulate the PI3K/Akt pathway. Consistent with the signaling pathway convergence, suppression of Alk and Pvr simultaneously or suppression of Alk/Pvr in *ptth* mutants exhibits prolonged delay of developmental timing and larger pupal size (Figures 1A and 1C–1E). In addition, activation of Alk/Pvr rescues the developmental defects of *ptth* mutants (Figures 4C and 4D), while activated Alk rescues the delay of InR^{DN} overexpression (Figure 3B). In total, both the downstream signaling pathway convergence and the additive effects of receptor activation/suppression support the coordination of signaling among these RTKs.

Cellular level coordination of receptor-mediated signals is very common during development. The PG is a good example of this coordination, which integrates a large variety of signals, such as insulin (Colombani et al., 2005; Mirth et al., 2005), PTTH (Shimell et al., 2018), Hedgehog (Palm et al., 2013; Rodenfels et al., 2014), Activin (Gibbens et al., 2011), BMP (Setiawan et al., 2018), serotonin (Shimada-Niwa and Niwa, 2014), and octopamine (Ohhara et al., 2015), to precisely control hormonal output. The coordination among receptors of the same class is of special interest. At least five RTKs (InR, Torso, Egfr, Alk, and Pvr) are expressed in the PG, all of which activate the Ras/Erk pathway (Cruz et al., 2020; Rewitz et al., 2009) (Figures 1B and 2C). Although PTTH/Torso has been considered the key tropic signal for PG function, it appears that three of the other RTKs can partially replace Torso to maintain some level of PG E production (Cruz et al., 2020; this study) Figures 1D and 1E). Loss of either the Torso, Alk, or Pvr signal causes developmental delay but does not block pupariation (Figures 1A and D). Even considering that loss of Egfr in the PG causes arrest at the L3 stage (Cruz et al., 2020), Egfr is still dispensable during the first two molts, which also require production of E pulses by the PG. These observations lead to an open question: why does the PG utilize multiple signals that appear to function redundantly?

An obvious possibility is that multiple timing signals provide both robustness and flexibility in response to variable developmental conditions. For example, given a choice of diets, *Drosophila* larvae chose one that maximizes developmental speed over other life-history traits (Rodrigues et al., 2015). This is not surprising given the ephemeral nature of rotting fruit, a primary food source for *Drosophila*. Thus, multiple signals may enable larvae to maximize developmental speed. Another possibility is that the different signals contribute to different temporal aspects of the developmental profile. For example, perhaps none of the receptors alone can achieve a strong enough Ras/Erk activation in late-stage larva that meets the demand for the large rise in E production that triggers wandering and initiation of pupation. Interestingly, the expression of Egfr (Cruz et al., 2020), Alk, and Pvr (Figure 1B) all increase remarkably during the late L3 stage when both Halloween gene expression and E synthesis ramps up, suggesting that the three receptors may function as supplements to Torso in order to achieve robust Ras/Erk activation and stimulation of E production.

Yet another possibility is that in addition to Ras/Erk signaling, each receptor may induce other downstream pathways. For instance, we have previously reported that regulated autophagy induction in the PG is a key mechanism that prevents precocious non-productive pupation by limiting E availability if larva have not achieved critical weight (CW) (Pan et al., 2019). In that report, we also demonstrated that after CW, autophagy inducibility is greatly repressed. This makes sense from a developmental perspective because if food becomes limiting after CW is achieved, it is likely disadvantageous to slow development down by limiting E production. Therefore, a mechanism to shut down autophagy inducibility after attainment of CW may be beneficial and, in this study, we found that Alk activation is, in part, responsible for shut down of autophagy activation in the PG after the CW nutrient checkpoint has been surpassed (Figures 3C–3E).

Activation of Alk/Pvr pathways results in dose-dependent effects on development via Jak/Stat signaling

Our manipulations of Alk and Pvr, but not Torso, signaling in the PG led to the discovery that Jak/Stat activation can also affect developmental timing (Figure S3B). A distinct feature of Alk and Pvr is that they can exert opposite effects on development likely depending on the activation strength. Weak activation of Alk or Pvr in the PG facilitates pupariation, while strong activation results in the arrest of development at various larval stages (Figures 4E and 4F) due to Jak/Stat activation. Using a weak *spok-Gal4* driver led to overgrowth of the PG and to atypical morphology (Figure S3A). Tissue overgrowth is commonly observed when either PI3K/Akt or Ras/Erk is hyperactivated in the PG; however, neither pathway induces atypical morphological change in the overgrown PGs or developmental arrest (Caldwell et al., 2005; Mirth et al., 2005), as we observe when Alk or Pvr are hyperactivated, especially with the strong *phm-Gal4* driver. Since suppression of Jak/Stat rescues the developmental arrest caused by *phm-Gal4*-driven Alk/Pvr hyperactivation (Figure 4G), it appears that Jak/Stat signaling is the key factor that mediates the side effect of Alk/Pvr activation on PG morphology and developmental timing. At lower levels of activation as found in the *spok>Alk*^{CA} and *spok>Pvr*^{CA}, many larvae still manage to pupariate (Figure 4A), suggesting that larvae can tolerate a certain level of ectopic Jak/Stat signaling caused by Alk/Pvr activation. What goes wrong at a high level of activation of Jak/Stat is still not clear.

At present, we do not know what the endogenous late Jak/Stat signal contributes in terms of PG function since knockdown with available reagents did not produce a significant phenotype (Figure 4G). In *Drosophila*, the canonical Jak/Stat signaling pathway is commonly induced by a group of cytokines including unpaired 1–3 (Upd1–3) via their cognate receptor Domeless (Dome) (Trivedi and Starz-Gaiano, 2018). However, it has also been reported that Torso and Pvr are capable of inducing Jak/Stat activation in some circumstances (Li et al., 2002; Mondal et al., 2011). Although we did not observe induction of Jak/Stat signal by overexpressing wild-type Torso in the PG (Figure S3B), this might be due to a weaker activation using wild-type Torso overexpression versus gain-of-function *tor*^{Y9} and *tor*^{RL3} mutants as used in the previous study (Li et al., 2002). Since we observed Dome expression and endogenous activation of the 10xStat92E-GFP reporter in late L3 PGs (Figure S3C), we assume that it is likely to play some role at this stage. Whether the Jak/Stat activation is through Alk/Pvr or via reception of canonical Upd/Dome signals

is not clear. Interestingly, note that Upd2 is secreted from the fat body into hemolymph (Rajan and Perrimon, 2012) and therefore may provide a nutrient storage signal to the PG that could be an important regulator of developmental timing, perhaps under certain types of non-standard laboratory growth conditions. It has also been recently demonstrated that inflammation-triggered release of Upd3 acts on the PG to produce developmental delay, indicating that the Jak/Stat pathway may be an important sensor for imbalance of various types of physiological processes (Romão et al., 2021).

Ligands activate Alk/Pvr through both neuronal and autocrine pathways

Since its discovery, PTTH has been recognized as the most important prothoracicotropic neuropeptide that triggers metamorphosis in holometabolous insects (Kawakami et al., 1990; McBrayer et al., 2007; Shimell et al., 2018; Smith and Rybczynski, 2012). In some species, such as *Bombyx mori*, additional prothoracicotropic neuropeptides such as orcokinin (Yamanaka et al., 2011) and FXPRL-amide peptides (Watanabe et al., 2007) have been discovered; however, PTTH, insulin-like peptides (Ilps), and serotonin (Shimada-Niwa and Niwa, 2014) are the only known brain-derived PG tropic hormones in *Drosophila*. Nevertheless, analysis of the *Drosophila ptth* null mutant phenotype verses PGN ablation and PGN electrical manipulation provided evidence that there are other tropic signals derived from the *Drosophila* PGNs (McBrayer et al., 2007; Shimell et al., 2018). Our observations described herein demonstrate that the Alk ligand Jeb and the Pvr ligand Pvf3 are produced in the PGNs (Figures 5A and 5B). Knockdown of *jeb* in the PGNs causes delay of pupariation and increased pupal size (Figures 5E and 5F), phenocopying the *phm>Alk*^{RNAi} animals (Figures 1A and 1C) and showing that the PGNs are the major source of Jeb that functions in the PG. Depletion of Pvf3 in the PGNs does not significantly affect developmental timing (Figures S3D and S3E), which is not a surprise since we found that Pvf2 and Pvf3 are also produced in the PG itself (Figures 5C and 5D). Overexpression of Jeb or *Pvf3* in the PGNs did not influence timing either (Figures S4J and S4K), indicating that the neural activity of PGNs and/or the temporal regulation of Alk/Pvr expression plays the dominant role in the regulation of signaling by these factors. We also point out that the combined knockdown of both *ptth* and *jeb* or *ptth*, *jeb*, and *Pvf3* in the PGNs still does not produce the ~4- to 5-day developmental delay exhibited by larvae in which the PGNs are ablated (Figure 5G versus Figure 5C in McBrayer et al. [2007]), likely signifying that the additional developmental delay produced by PGN ablation is due to elimination of some other non-RTK-mediated neuropeptide signals.

Besides the well-established role of the PGNs in regulating developmental timing and body size, several recent studies also indicate that autocrine signaling within the PG itself provides important developmental regulatory cues. This was first documented for biogenic amine signaling (Ohhara et al., 2015) but more recently was extended to include the RTK Egfr and its ligands Vein and Spitz (Cruz et al., 2020). Interestingly, the expression levels of Vein and Spitz in the PG increase in middle to late L3 and may not contribute to CW determination, but instead they respond to it to form part of a E feedforward circuit that helps ramp up hormone production during late L3 in anticipation of the large pulse that drives pupation (Cruz et al., 2020; Moeller et al., 2013). Similarly, since we observe expression of both *Pvf2* and *Pvf3* in the late L3 PG (Figures 5C and 5D), and since

knockdown of *Pvf2* and *Pvf3* simultaneously in the PG causes delay of pupariation and larger pupal size (Figure 5I and J), these ligands together with their receptor Pvr also appear to form an autocrine signaling pathway. We and others have also observed expression of *Pvf2/3* in other tissues/cell types such as fat body, salivary gland (data not shown), and hemocytes (Parsons and Foley, 2013). Whether these sources also provide some input to the PG is not clear. We also found that overexpression of Pvf2 or Pvf3 did not cause accelerated development (Figures S4L and S4M), which is in stark contrast to the case of Egfr signaling in which overexpression of Vein or Spitz advances pupariation significantly (Cruz et al., 2020). This finding indicates that the activity of Pvr signaling may depend on the expression of Pvr receptor and/or the release of ligands, rather than ligand expression. Endogenous *Pvf2* expression is limited to the late L3 stage, yet *Pvf3* is constitutively expressed in the L3 stage (Figures 5C and 5D). The biological significance of the differentially regulated Pvf ligand expression is still an open question. It is noteworthy that there are three Pvr isoforms produced by alternative splicing among the exons coding the ligand-binding domain (Cho et al., 2002; Hoch and Soriano, 2003). Thus, reception of different Pvf ligand signals could very much depend on the levels and timing of receptor isoform expression in the PG. Lastly, we note that neither Alk nor Pvr accumulates to substantial levels on the PG membrane until after CW (Figure 1B). Thus, similar to Egfr signaling, their primary functions likely control post-CW events. What regulates the post-CW membrane localization of these receptors is not yet clear, but it is interesting to speculate that the process might be one of the first downstream responses to surpassing the CW checkpoint that prepares the PG gland for a major acceleration in hormone production.

STAR★METHODS

RESOURCE AVAILABILITY

Lead contact—Further information and requests for resources and reagents should be directed to and will be fulfilled by the lead contact, Michael B. O'Connor (moconnor@umn.edu).

Materials availability—Three *T2A-Gal4* fly lines, jeb^{T2A}*-Gal4,* $Pvf2^{T2A}$*-Gal4* and $Pvf3^{T2A}$*-Gal4*, are generated in this study. The request for the fly lines should be directed to the lead contact.

Data and code availability—All data reported in this paper will be shared by the lead contact upon request. This paper does not report original code. Any additional information required to reanalyze the data reported in this paper is available from the lead contact upon request.

EXPERIMENTAL MODEL AND SUBJECT DETAILS

Flies—Unless noted, all flies were reared on standard agar-cornmeal food supplemented with yeast at 25 °C. Flies were cultured in 12:12 light-dark cycles, however, all experiments were carried out under constant light to avoid the potential impact of circadian cycle on developmental timing. *Phm-Gal4* (Ono et al., 2006) and *spok-Gal4* (Moeller et al., 2017) was used to drive gene expression specifically in PG cells. *NP423-Gal4* (Yamanaka et

al., 2013b) was used to drive gene expression in the PGNs. *Dome-Gal4* (Ghiglione et al., 2002) (gift from Dr. Norbert Perrimon) was used to examine the expression of *Domeless* in the PG. *Spok*^{GeneSwitch}*-Gal4* (Zeng et al., 2020) was used to drive temporally specific gene expression under control of RU486 administration. A collection of RNAi strains from Transgenic RNAi Project (TRiP) (Ni et al., 2011) were obtained from Bloomington Stock Center (BDSC) and used to carry out the targeted screen of RTKs (see STAR methods). Additional RNAi lines used for gene knockdown were obtained from BDSC, Vienna *Drosophila* Resource Center (VDRC) and National Institute of Genetics (NIG), Japan. *UAS-Alk*^{CA} (Zettervall et al., 2004), *UAS-Alk*^{DN} (Bazigou et al., 2007) and *UAS-jeb* (Varshney and Palmer, 2006) lines (gifts from Dr. Ruth Palmer) were used to manipulate Alk signaling. *UAS-Pvr* (BDSC #58998), *UAS-Pvr*^{CA} (BDSC #58428), *UAS-Pvr*^{DN} (BDSC #58431), *UAS-Pvf2* and *UAS-Pvf3* lines (gifts from Dr. Edan Foley) were used to manipulate Pvr signaling. UAS-Torso and *UAS-InR*^{CA} (BDSC #8440) lines were used to manipulate Torso and InR signaling, respectively. *tGPH* (BDSC #8163) and *10xStat92E-GFP* (BDSC #26197) lines were used to monitor activation of Pi3K/Akt and Jak/Stat pathway, respectively. *jeb*^{T2A}*-Gal4*, *Pvf2*^{T2A}*-Gal4* and *Pvf3*^{T2A}*-Gal4* lines were generated from *jeb*^{MI03124} (BDSC #36200), *Pvf2*^{MI00770} (BDSC #32696) and *Pvf3*^{MI04168} (BDSC #37270), respectively, following recombinase-mediated cassette exchange strategy (Diao et al., 2015) and were used to examine the expression pattern of the corresponding genes. *ptth*^{120F2A} (Shimell et al., 2018) and *Pvf1*^{EP1624} (BDSC #11450) null mutant lines were also used in the study.

METHOD DETAILS

Developmental timing measurement—Before egg collection, flies were transferred to constant light environment for at least 2 days and all subsequent treatments were carried out under constant light. Eggs were collected on apple juice plates with yeast paste and early L1 larvae were transferred to standard lab fly food with yeast paste after 24 hr. After larvae enter wandering stage, the number of pupa was counted every 6 hours until all larvae pupariated.

Pupal volume measurement—Pupae were picked from vials and imaged under dissection stereoscope. The length (L) and width (W) of pupae were measured using ImageJ software, and the pupal volume (V) was calculated in Microsoft Excel using the following equation,

$$V = 4/3 * \pi * (W/2)^2 * (L/2).$$

Volumes were then normalized to the average volume of control and the "Δ pupal volumes" were presented in figures.

Fluorescence microscopy—Larvae were dissected in PBS and fixed using 3.7% formaldehyde for 15 mins at room temperature. Tissues were then washed in PBS and mounted in 90% glycerol for imaging. All confocal images were captured using Zeiss LSM710 confocal microscope.

Immunohistochemistry—Larvae were dissected in PBS and fixed using 3.7% formaldehyde for 30 mins at room temperature. Tissues were washed in PBS containing 0.1% Triton X-100 (PBT) for 3 times and then permeabilized and blocked simultaneously using PBT containing 5% normal goat serum (NGS) for 1 hour. Tissues were then incubated with primary antibody (anti-Alk, 1:1000, anti-Pvr, 1:100, anti-phospho-Erk, 1:200) in PBT containing 10% NGS overnight at 4 degrees, followed by 5 washes and then post-secondary incubation for 2 hours at room temperature. DAPI staining occurred for 5 minutes at the pen-ultimate washing step after secondary antibody incubation. Finally, tissues were transferred to 70% glycerol/PBS mounting medium and then mounted on glass slide for imaging. Images were captured using a Zeiss LSM 710 confocal microscope.

Fluorescence *in situ* hybridization (FISH) of neuropeptide ligands

Preparation of anti-sense probes: The FISH Tag RNA Multicolor Kit (Invitrogen) protocol was used to prepare fluorescence-labeled probes for *in situ* hybridization. *Ptth* (Clone ID: IP07658) and *jeb* (Clone ID: GH16255) were cut and transcribed with Sp6 to make anti-sense message. One μg of amine-modified RNA was labeled with either Alexa Fluor® 488 or Alexa Fluor®®594. The fluorescent-tagged RNA was then fragmented to yield ~300 bp fragments (Kosman et al., 2004), precipitated, and resuspended in hybridization solution (50% formamide, 5x SSC, 50 μg/mL heparin, 100 μg/mL salmon sperm DNA, 0.2% Triton X-100) at a concentration of 10 ng/μL.

In situ hybridization: A mix of early, middle, and late third instar larvae were fixed for 20 minutes, washed with PBTr (PBS + 0.2% Triton X-100), and then treated with 5 μg/mL proteinase K for 5 minutes. After washing with PBTr, the larvae were transitioned to hybridization solution (Kosman et al., 2004) and pre-hybridized for 1 hour at 55°C. Hybridization solution (100 μL) containing fluorescent probes was denatured at 85°C for 3 minutes, chilled on ice, and then added to pre-hybridized larvae. After hybridization at 55°C for 21 hours, larvae were washed 4 times in hybridization solution at 55°C (one of these overnight), transitioned out of hybridization solution to PBTr, washed in PBTr and then placed in 80% glycerol, 20% PBTr for imaging.

Ecdysteroid titer measurement—The ecdysteroid titers of larvae were measured using the 20-hydroxyecdysone Enzyme Immunoassay (EIA) kit (Cayman Chemicals), which detects both ecdysone (E) and 20-hydroxyecdysone (20E). Briefly, frozen larvae were homogenized in methanol and ecdysteroids were extracted as described previously (Warren et al., 2006). The extracts were evaporated in a Speed Vac and the residue resuspended in EIA buffer and analyzed following the manufacturer's protocol. A standard curve was determined using a dilution series containing a known amount of purified 20E solution provided by the kit. Absorbance at 415 nm was detected using a benchtop microplate reader (Bio-Rad).

Quantitative RT-PCR (qRT-PCR)—Larvae were washed in PBS and then homogenized in Trizol (Invitrogen). Total RNA was purified using RNeasy Mini Kit (QIAGEN) and cDNA library was obtained using SuperScript-III (Invitrogen) following the manufacturer's protocol. qRT-PCR was then carried out using SYBR Green reagent (Roche) on a

LightCycler 480 platform. *Rpl23* was used as internal control for normalization. Primers used in this study are listed below.

Rpl23 F 5′- GACAACACCGGAGCCAAGAACC –3′

R 5′- GTTTGCGCTGCCGAATAACCAC –3′

nvd F 5′- GGAAGCGTTGCTGACGACTGTG –3′

R 5′- TAAAGCCGTCCACTTCCTGCGA –3′

spok F 5′- TATCTCTTGGGCACACTCGCTG –3′

R 5′- GCCGAGCTAAATTTCTCCGCTT –3′

sro F 5′- CCACAACATCAAGTCGGAAGGAGC –3′

R 5′- ACCAGGCGAATGGAATCGGG –3′

Cyp6t3 F 5′- GGTGTGTTTGGAGGCACTG –3′

R 5′- GGTGCACTCTCTGTTGACGA –3′

phm F 5′- GGATTTCTTTCGGCGCGATGTG –3′

R 5′- TGCCTCAGTATCGAAAAGCGGT –3′

dib F 5′- TGCCCTCAATCCCTATCTGGTC –3′

R 5′- ACAGGGTCTTCACACCCATCTC –3′

sad F 5′- CCGCATTCAGCAGTCAGTGG –3′

R 5′- ACCTGCCGTGTACAAGGAGAG –3′

QUANTIFICATION AND STATISTICAL ANALYSIS

Quantification of autophagic vesicles—The number and area of Atg8a positive vesicles were quantified using imageJ software. Briefly, the vesicles were selected using the "threshold" function. Then the number and total area of the vesicles were calculated automatically using the "analyze particles" function in the software.

Statistics—GraphPad Prism software was used to carry out statistical analyses and Student's t test was used to determine statistical significance. For all graphs, the numbers of replicates (n values) can be found in the corresponding figure legends. All graphs represent mean values ± SEM, while the p values in the graphs indicate: *$p < 0.05$, **$p < 0.01$ ***$p < 0.001$ and ****$p < 0.0001$.

Supplementary Material

Refer to Web version on PubMed Central for supplementary material.

ACKNOWLEDGMENTS

We thank Dr. Ruth Palmer, Dr. Edan Foley, Dr. Norbert Perrimon, and Dr. Ben-Zion Shilo for fly line and reagent sharing. We thank MaryJane Shimell for preforming the *in situ jeb* and *Pvf2/3* hybridization experiments. We also thank the Vienna Drosophila RNAi Center, the Bloomington Drosophila Stock Center, and the National Institute of Genetics in Japan for fly stocks. This work was supported by grant 1R35GM118029 from NIGMS to M.B.O.

REFERENCES

Bazigou E, Apitz H, Johansson J, Lorén CE, Hirst EM, Chen PL, Palmer RH, and Salecker I (2007). Anterograde Jelly belly and Alk receptor tyrosine kinase signaling mediates retinal axon targeting in *Drosophila*. Cell 128, 961–975. [PubMed: 17350579]

Caldwell PE, Walkiewicz M, and Stern M (2005). Ras activity in the *Drosophila* prothoracic gland regulates body size and developmental rate via ecdysone release. Curr. Biol 15, 1785–1795. [PubMed: 16182526]

Callier V, and Nijhout HF (2013). Body size determination in insects: A review and synthesis of size- and brain-dependent and independent mechanisms. Biol. Rev. Camb. Philos. Soc 88, 944–954. [PubMed: 23521745]

Cheng LY, Bailey AP, Leevers SJ, Ragan TJ, Driscoll PC, and Gould AP (2011). Anaplastic lymphoma kinase spares organ growth during nutrient restriction in *Drosophila*. Cell 146, 435–447. [PubMed: 21816278]

Cho NK, Keyes L, Johnson E, Heller J, Ryner L, Karim F, and Krasnow MA (2002). Developmental control of blood cell migration by the *Drosophila* VEGF pathway. Cell 108, 865–876. [PubMed: 11955438]

Colombani J, Bianchini L, Layalle S, Pondeville E, Dauphin-Villemant C, Antoniewski C, Carré C, Noselli S, and Léopold P (2005). Antagonistic actions of ecdysone and insulins determine final size in *Drosophila*. Science 310, 667–670. [PubMed: 16179433]

Colombani J, Andersen DS, and Léopold P (2012). Secreted peptide Dilp8 coordinates *Drosophila* tissue growth with developmental timing. Science 336, 582–585. [PubMed: 22556251]

Colombani J, Andersen DS, Boulan L, Boone E, Romero N, Virolle V, Texada M, and Léopold P (2015). *Drosophila* Lgr3 couples organ growth with maturation and ensures developmental stability. Curr. Biol 25, 2723–2729. [PubMed: 26441350]

Cruz J, Martin D, and Franch-Marro X (2020). Egfr signaling is a major regulator of ecdysone biosynthesis in the Drosophila prothoracic gland. Curr. Biol 30, 1547–1554.e4. [PubMed: 32220314]

Danielsen ET, Moeller ME, Yamanaka N, Ou Q, Laursen JM, Soenderholm C, Zhuo R, Phelps B, Tang K, Zeng J, et al. (2016). A *Drosophila* genome-wide screen identifies regulators of steroid hormone production and developmental timing. Dev. Cell 37, 558–570. [PubMed: 27326933]

Deveci D, Martin FA, Leopold P, and Romero NM (2019). AstA signaling functions as an evolutionary conserved mechanism timing juvenile to adult transition. Curr. Biol 29, 813–822.e4. [PubMed: 30799245]

Diao F, Ironfield H, Luan H, Diao F, Shropshire WC, Ewer J, Marr E, Potter CJ, Landgraf M, and White BH (2015). Plug-and-play genetic access to Drosophila cell types using exchangeable exon cassettes. Cell Rep. 10, 1410–1421. [PubMed: 25732830]

Duchek P, Somogyi K, Jékely G, Beccari S, and Rørth P (2001). Guidance of cell migration by the *Drosophila* PDGF/VEGF receptor. Cell 107, 17–26. [PubMed: 11595182]

Englund C, Lorén CE, Grabbe C, Varshney GK, Deleuil F, Hallberg B, and Palmer RH (2003). Jeb signals through the Alk receptor tyrosine kinase to drive visceral muscle fusion. Nature 425, 512–516. [PubMed: 14523447]

Garelli A, Gontijo AM, Miguela V, Caparros E, and Dominguez M (2012). Imaginal discs secrete insulin-like peptide 8 to mediate plasticity of growth and maturation. Science 336, 579–582. [PubMed: 22556250]

Garelli A, Heredia F, Casimiro AP, Macedo A, Nunes C, Garcez M, Dias ARM, Volonte YA, Uhlmann T, Caparros E, et al. (2015). Dilp8 requires the neuronal relaxin receptor Lgr3 to couple growth to developmental timing. Nat. Commun 6, 8732. [PubMed: 26510564]

Ghiglione C, Devergne O, Georgenthum E, Carballès F, Médioni C, Cerezo D, and Noselli S (2002). The *Drosophila* cytokine receptor Domeless controls border cell migration and epithelial polarization during oogenesis. Development 129, 5437–5447. [PubMed: 12403714]

Ghosh A, McBrayer Z, and O'Connor MB (2010). The *Drosophila* gap gene *giant* regulates ecdysone production through specification of the PTTH-producing neurons. Dev. Biol 347, 271–278. [PubMed: 20816678]

Gibbens YY, Warren JT, Gilbert LI, and O'Connor MB (2011). Neuroendocrine regulation of *Drosophila* metamorphosis requires TGFβ/Activin signaling. Development 138, 2693–2703. [PubMed: 21613324]

Gouzi JY, Moressis A, Walker JA, Apostolopoulou AA, Palmer RH, Bernards A, and Skoulakis EM (2011). The receptor tyrosine kinase Alk controls neurofibromin functions in Drosophila growth and learning. PLoS Genet. 7, e1002281. [PubMed: 21949657]

Hill RJ, Billas IM, Bonneton F, Graham LD, and Lawrence MC (2013). Ecdysone receptors: From the Ashburner model to structural biology. Annu. Rev. Entomol 58, 251–271. [PubMed: 23072463]

Hoch RV, and Soriano P (2003). Roles of PDGF in animal development. Development 130, 4769–4784. [PubMed: 12952899]

Imura E, Shimada-Niwa Y, Nishimura T, Hückesfeld S, Schlegel P, Ohhara Y, Kondo S, Tanimoto H, Cardona A, Pankratz MJ, and Niwa R (2020). The Corazonin-PTTH neuronal axis controls systemic body growth by regulating basal ecdysteroid biosynthesis in *Drosophila melanogaster*. Curr. Biol 30, 2156–2165.e5. [PubMed: 32386525]

Kawakami A, Kataoka H, Oka T, Mizoguchi A, Kimura-Kawakami M, Adachi T, Iwami M, Nagasawa H, Suzuki A, and Ishizaki H (1990). Molecular cloning of the Bombyx mori prothoracicotropic hormone. Science 247, 1333–1335. [PubMed: 2315701]

Kosman D, Mizutani CM, Lemons D, Cox WG, McGinnis W, and Bier E (2004). Multiplex detection of RNA expression in *Drosophila* embryos. Science 305, 846. [PubMed: 15297669]

Learte AR, Forero MG, and Hidalgo A (2008). Gliatrophic and gliatropic roles of PVF/PVR signaling during axon guidance. Glia 56, 164–176. [PubMed: 18000865]

Li WX, Agaisse H, Mathey-Prevot B, and Perrimon N (2002). Differential requirement for STAT by gain-of-function and wild-type receptor tyrosine kinase Torso in *Drosophila*. Development 129, 4241–4248. [PubMed: 12183376]

Li-Kroeger D, Kanca O, Lee PT, Cowan S, Lee MT, Jaiswal M, Salazar JL, He Y, Zuo Z, and Bellen HJ (2018). An expanded toolkit for gene tagging based on MiMIC and scarless CRISPR tagging in *Drosophila*. eLife 7, e38709. [PubMed: 30091705]

Lorén CE, Scully A, Grabbe C, Edeen PT, Thomas J, McKeown M, Hunter T, and Palmer RH (2001). Identification and characterization of DAlk: A novel *Drosophila melanogaster* RTK which drives ERK activation in vivo. Genes Cells 6, 531–544. [PubMed: 11442633]

McBrayer Z, Ono H, Shimell M, Parvy JP, Beckstead RB, Warren JT, Thummel CS, Dauphin-Villemant C, Gilbert LI, and O'Connor MB (2007). Prothoracicotropic hormone regulates developmental timing and body size in *Drosophila*. Dev. Cell 13, 857–871. [PubMed: 18061567]

Mele S, and Johnson TK (2019). Receptor tyrosine kinases in development: Insights from *Drosophila*. Int. J. Mol. Sci 21, 188.

Mirth C, Truman JW, and Riddiford LM (2005). The role of the prothoracic gland in determining critical weight for metamorphosis in *Drosophila melanogaster*. Curr. Biol 15, 1796–1807. [PubMed: 16182527]

Moeller ME, Danielsen ET, Herder R, O'Connor MB, and Rewitz KF (2013). Dynamic feedback circuits function as a switch for shaping a maturation-inducing steroid pulse in *Drosophila*. Development 140, 4730–4739. [PubMed: 24173800]

Moeller ME, Nagy S, Gerlach SU, Soegaard KC, Danielsen ET, Texada MJ, and Rewitz KF (2017). Warts signaling controls organ and body growth through regulation of ecdysone. Curr. Biol 27, 1652–1659.e4. [PubMed: 28528906]

Mondal BC, Mukherjee T, Mandal L, Evans CJ, Sinenko SA, Martinez-Agosto JA, and Banerjee U (2011). Interaction between differentiating cell- and niche-derived signals in hematopoietic progenitor maintenance. Cell 147, 1589–1600. [PubMed: 22196733]

Nagarkar-Jaiswal S, Lee PT, Campbell ME, Chen K, Anguiano-Zarate S, Gutierrez MC, Busby T, Lin WW, He Y, Schulze KL, et al. (2015). A library of MiMICs allows tagging of genes and reversible, spatial and temporal knockdown of proteins in Drosophila. eLife 4, e05338.

Ni JQ, Zhou R, Czech B, Liu LP, Holderbaum L, Yang-Zhou D, Shim HS, Tao R, Handler D, Karpowicz P, et al. (2011). A genome-scale shRNA resource for transgenic RNAi in *Drosophila*. Nat. Methods 8, 405–407. [PubMed: 21460824]

Niwa R, and Niwa YS (2014). Enzymes for ecdysteroid biosynthesis: Their biological functions in insects and beyond. Biosci. Biotechnol. Biochem 78, 1283–1292. [PubMed: 25130728]

Ohhara Y, Shimada-Niwa Y, Niwa R, Kayashima Y, Hayashi Y, Akagi K, Ueda H, Yamakawa-Kobayashi K, and Kobayashi S (2015). Autocrine regulation of ecdysone synthesis by β3-octopamine receptor in the prothoracic gland is essential for *Drosophila* metamorphosis. Proc. Natl. Acad. Sci. USA 112, 1452–1457. [PubMed: 25605909]

Okamoto N, Viswanatha R, Bittar R, Li Z, Haga-Yamanaka S, Perrimon N, and Yamanaka N (2018). A membrane transporter is required for steroid hormone uptake in *Drosophila*. Dev. Cell 47, 294–305.e7. [PubMed: 30293839]

Ono H, Rewitz KF, Shinoda T, Itoyama K, Petryk A, Rybczynski R, Jarcho M, Warren JT, Marqués G, Shimell MJ, et al. (2006). *Spook* and *Spookier* code for stage-specific components of the ecdysone biosynthetic pathway in Diptera. Dev. Biol 298, 555–570. [PubMed: 16949568]

Palm W, Swierczynska MM, Kumari V, Ehrhart-Bornstein M, Bornstein SR, and Eaton S (2013). Secretion and signaling activities of lipoprotein-associated Hedgehog and non-sterol-modified Hedgehog in flies and mammals. PLoS Biol. 11, e1001505. [PubMed: 23554573]

Pan X, Neufeld TP, and O'Connor MB (2019). A tissue- and temporal-specific autophagic switch controls *Drosophila* pre-metamorphic nutritional checkpoints. Curr. Biol 29, 2840–2851.e4. [PubMed: 31422886]

Parsons B, and Foley E (2013). The *Drosophila* platelet-derived growth factor and vascular endothelial growth factor-receptor related (Pvr) protein ligands Pvf2 and Pvf3 control hemocyte viability and invasive migration. J. Biol. Chem 288, 20173–20183. [PubMed: 23737520]

Petryk A, Warren JT, Marqués G, Jarcho MP, Gilbert LI, Kahler J, Parvy JP, Li Y, Dauphin-Villemant C, and O'Connor MB (2003). Shade is the *Drosophila* P450 enzyme that mediates the hydroxylation of ecdysone to the steroid insect molting hormone 20-hydroxyecdysone. Proc. Natl. Acad. Sci. USA 100, 13773–13778. [PubMed: 14610274]

Rajan A, and Perrimon N (2012). *Drosophila* cytokine unpaired 2 regulates physiological homeostasis by remotely controlling insulin secretion. Cell 151, 123–137. [PubMed: 23021220]

Rewitz KF, Yamanaka N, Gilbert LI, and O'Connor MB (2009). The insect neuropeptide PTTH activates receptor tyrosine kinase Torso to initiate metamorphosis. Science 326, 1403–1405. [PubMed: 19965758]

Rodenfels J, Lavrynenko O, Ayciriex S, Sampaio JL, Carvalho M, Shevchenko A, and Eaton S (2014). Production of systemically circulating Hedgehog by the intestine couples nutrition to growth and development. Genes Dev. 28, 2636–2651. [PubMed: 25452274]

Rodrigues MA, Martins NE, Balancé LF, Broom LN, Dias AJ, Fernandes AS, Rodrigues F, Sucena É, and Mirth CK (2015). *Drosophila melanogaster* larvae make nutritional choices that minimize developmental time. J. Insect Physiol 81, 69–80. [PubMed: 26149766]

Roman G, Endo K, Zong L, and Davis RL (2001). P{Switch}, a system for spatial and temporal control of gene expression in *Drosophila melanogaster*. Proc. Natl. Acad. Sci. USA 98, 12602–12607. [PubMed: 11675496]

Romão D, Muzzopappa M, Barrio L, and Milán M (2021). The Upd3 cytokine couples inflammation to maturation defects in *Drosophila*. Curr. Biol 31, 1780–1787.e6. [PubMed: 33609452]

Sansone CL, Cohen J, Yasunaga A, Xu J, Osborn G, Subramanian H, Gold B, Buchon N, and Cherry S (2015). Microbiota-dependent priming of antiviral intestinal immunity in *Drosophila*. Cell Host Microbe 18, 571–581. [PubMed: 26567510]

Setiawan L, Pan X, Woods AL, O'Connor MB, and Hariharan IK (2018). The BMP2/4 ortholog Dpp can function as an inter-organ signal that regulates developmental timing. Life Sci. Alliance 1, e201800216. [PubMed: 30515478]

Shimada-Niwa Y, and Niwa R (2014). Serotonergic neurons respond to nutrients and regulate the timing of steroid hormone biosynthesis in *Drosophila*. Nat. Commun 5, 5778. [PubMed: 25502946]

Shimell M, Pan X, Martin FA, Ghosh AC, Leopold P, O'Connor MB, and Romero NM (2018). Prothoracicotropic hormone modulates environmental adaptive plasticity through the control of developmental timing. Development 145, dev159699.

Smith W, and Rybczynski R (2012). Prothoracicotropic hormone. In Insect Endocrinology, Gibert LI, ed. (Elsevier), pp. 1–62.

Texada MJ, Malita A, Christensen CF, Dall KB, Faergeman NJ, Nagy S, Halberg KA, and Rewitz K (2019). Autophagy-mediated cholesterol trafficking controls steroid production. Dev. Cell 48, 659–671.e4. [PubMed: 30799225]

Trivedi S, and Starz-Gaiano M (2018). *Drosophila* Jak/STAT signaling: Regulation and relevance in human cancer and metastasis. Int. J. Mol. Sci 19, 4056.

Uchibori-Asano M, Kayukawa T, Sezutsu H, Shinoda T, and Daimon T (2017). Severe developmental timing defects in the prothoracicotropic hormone (PTTH)-deficient silkworm, Bombyx mori. Insect Biochem. Mol. Biol 87, 14–25. [PubMed: 28627423]

Vallejo DM, Juarez-Carreño S, Bolivar J, Morante J, and Dominguez M (2015). A brain circuit that synchronizes growth and maturation revealed through Dilp8 binding to Lgr3. Science 350, aac6767.

Varshney GK, and Palmer RH (2006). The bHLH transcription factor Hand is regulated by Alk in the *Drosophila* embryonic gut. Biochem. Biophys. Res. Commun 351, 839–846. [PubMed: 17094947]

Warren JT, Yerushalmi Y, Shimell MJ, O'Connor MB, Restifo LL, and Gilbert LI (2006). Discrete pulses of molting hormone, 20-hydroxyecdysone, during late larval development of *Drosophila melanogaster*: Correlations with changes in gene activity. Dev. Dyn 235, 315–326. [PubMed: 16273522]

Watanabe K, Hull JJ, Niimi T, Imai K, Matsumoto S, Yaginuma T, and Kataoka H (2007). FXPRL-amide peptides induce ecdysteroidogenesis through a G-protein coupled receptor expressed in the prothoracic gland of *Bombyx mori*. Mol. Cell. Endocrinol 273, 51–58. [PubMed: 17590269]

Weinkove D, and Leevers SJ (2000). The genetic control of organ growth: Insights from *Drosophila*. Curr. Opin. Genet. Dev 10, 75–80. [PubMed: 10679387]

Wu M, Pastor-Pareja JC, and Xu T (2010). Interaction between Ras^{V12} and *scribbled* clones induces tumour growth and invasion. Nature 463, 545–548. [PubMed: 20072127]

Yamanaka N, Roller L, Zitňan D, Satake H, Mizoguchi A, Kataoka H, and Tanaka Y (2011). *Bombyx* orcokinins are brain-gut peptides involved in the neuronal regulation of ecdysteroidogenesis. J. Comp. Neurol 519, 238–246. [PubMed: 21165973]

Yamanaka N, Rewitz KF, and O'Connor MB (2013a). Ecdysone control of developmental transitions: Lessons from *Drosophila* research. Annu. Rev. Entomol 58, 497–516. [PubMed: 23072462]

Yamanaka N, Romero NM, Martin FA, Rewitz KF, Sun M, O'Connor MB, and Léopold P (2013b). Neuroendocrine control of *Drosophila* larval light preference. Science 341, 1113–1116. [PubMed: 24009394]

Yamanaka N, Marqués G, and O'Connor MB (2015). Vesicle-mediated steroid hormone secretion in *Drosophila melanogaster*. Cell 163, 907–919. [PubMed: 26544939]

Zeng J, Huynh N, Phelps B, and King-Jones K (2020). Snail synchronizes endocycling in a TOR-dependent manner to coordinate entry and escape from endoreplication pausing during the *Drosophila* critical weight checkpoint. PLoS Biol. 18, e3000609. [PubMed: 32097403]

Zettervall CJ, Anderl I, Williams MJ, Palmer R, Kurucz E, Ando I, and Hultmark D (2004). A directed screen for genes involved in *Drosophila* blood cell activation. Proc. Natl. Acad. Sci. USA 101, 14192–14197. [PubMed: 15381778]

Highlights

- Juxtacrine Jeb/Alk and autocrine Pvf/Pvr signals control timing of ecdysone production
- Jeb/Alk and Pvf/Pvr augment PTTH/Torso and EGFR signaling, respectively, via Ras/Erk
- Jeb/Alk signaling also regulates starvation-induced autophagy within the PG
- Jeb/Alk and Pvf/Pvr can also dose-dependently activate the Jak/Stat pathway in the PG

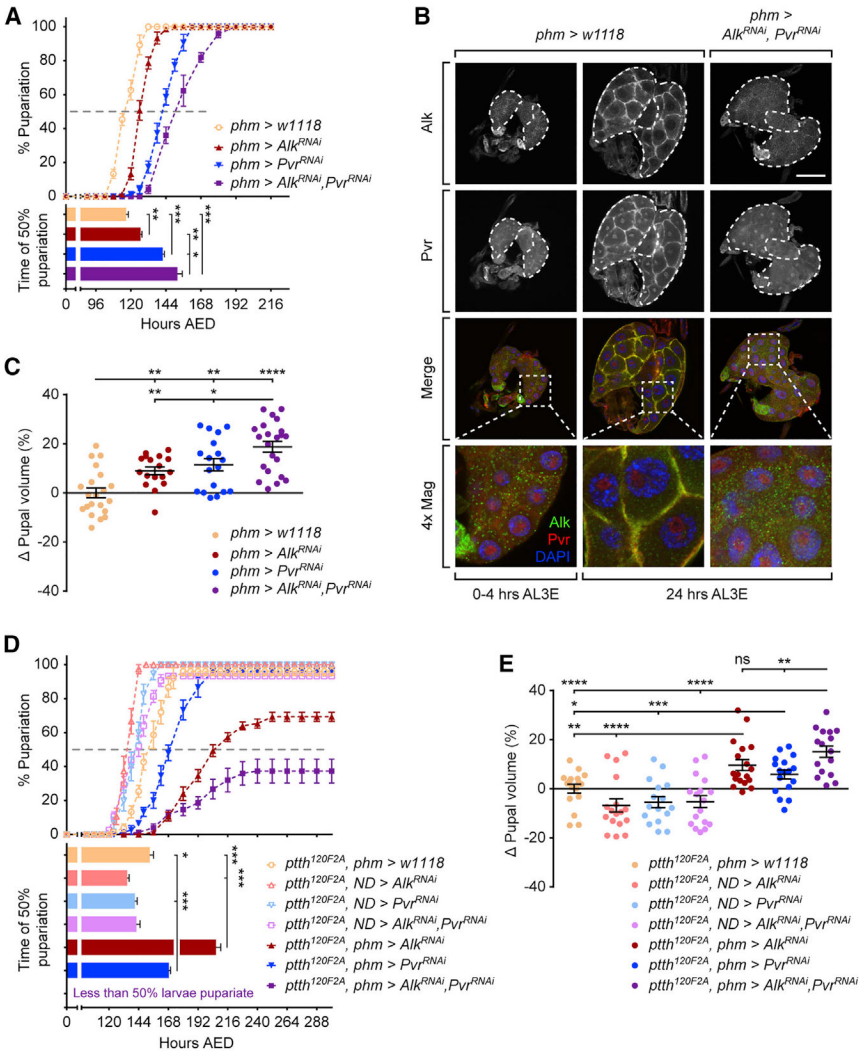

Figure 1. Alk and Pvr regulate developmental timing and body size in coordination with PTTH/Torso pathway

(A) Pupariation timing curves and the time of 50% pupariation of *phm>w1118*, *phm>Alk^{RNAi}*, *phm>Pvr^{RNAi}*, and *phm>Alk^{RNAi},Pvr^{RNAi}* larvae.

(B) Immunofluorescence images of *phm>w1118* and *phm>Alk^{RNAi},Pvr^{RNAi}* PGs stained with anti-Alk and anti-Pvr antibodies. Images of *phm>w1118* PGs show the changes in Alk and Pvr immunofluorescence signals on the cell membrane, and images of *phm>Alk^{RNAi},Pvr^{RNAi}* PG show that the cytoplasmic signal is non-specific. Dash lines outline the PG area of the ring gland. Scale bar, 50 μm.

(C) Relevant pupal volume changes in animals tested in (A).

(D) Pupariation timing curves and the time of 50% pupariation of *phm>w1118*, *phm>Alk^{RNAi}*, *phm>Pvr^{RNAi}*, and *phm>Alk^{RNAi},Pvr^{RNAi}* larvae with *ptth^{120F2A}* mutant background. ND, no driver.

(E) Relevant pupal volume changes in animals tested in (D).

(A and C–E) Mean ± SEM; p values by unpaired t test (n = 3 in A and D, n = 17–22 in C and E; *p < 0.05, **p < 0.01, ***p < 0.001, ****p < 0.0001; ns, not significant).

See also Figure S1.

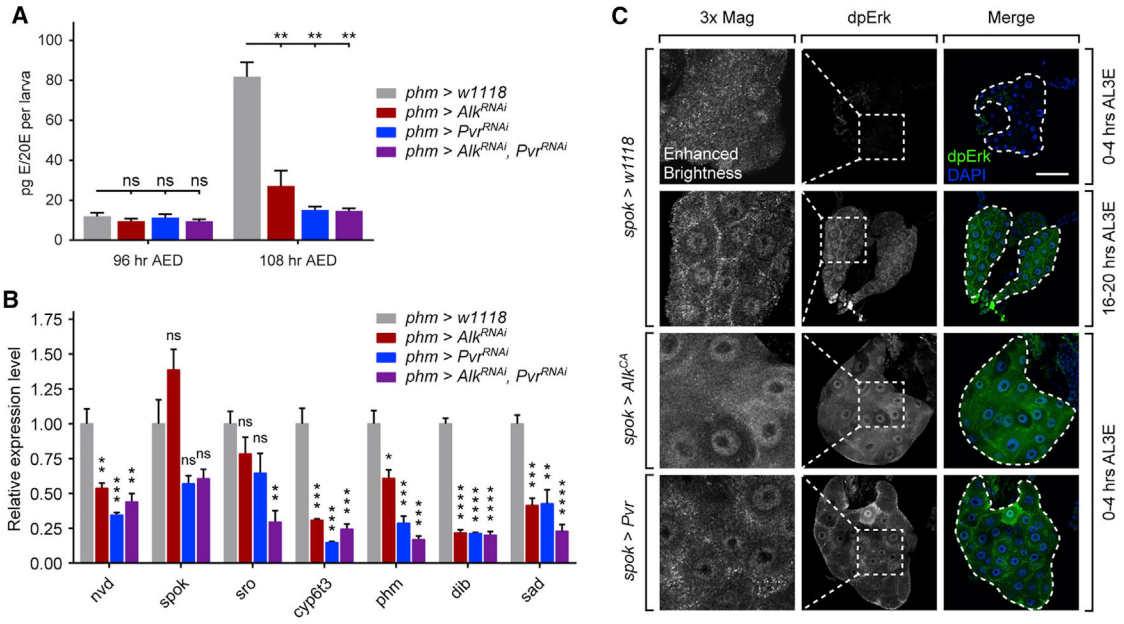

Figure 2. Alk and Pvr facilitate ecdysone synthesis and Halloween gene expression by activating the Ras/Erk pathway

(A) Quantification of ecdysone/20-hydroxyecdysone titers in *phm>w1118*, *phm>Alk*^{RNAi}, *phm>Pvr*^{RNAi}, and *phm>Alk*^{RNAi},*Pvr*^{RNAi} larvae at indicated timing stages.

(B) qRT-PCR measurements of Halloween gene expressions in wandering *phm>w1118* and age-matched *phm>Alk*^{RNAi}, *phm>Pvr*^{RNAi} and *phm>Alk*^{RNAi},*Pvr*^{RNAi} larvae.

(A and B) Mean ± SEM; p values by unpaired t test (n = 3 in A, n = 4 in B; *p < 0.05, **p < 0.01, ***p < 0.001, ****p < 0.0001).

(C) Immunofluorescence images of *spok>w1118*, *spok>Alk*^{CA}, and *spok>Pvr* PGs stained with anti-phospho-Erk antibody. Dash lines outline the PG area of the ring gland in the right lane. Enlarged images of the indicated areas are shown in the left lane. To visualize the distribution of fluorescence signals in early L3 *spok>w1118* larvae, the brightness is enhanced in the enlarged image. Scale bar, 50 μm.

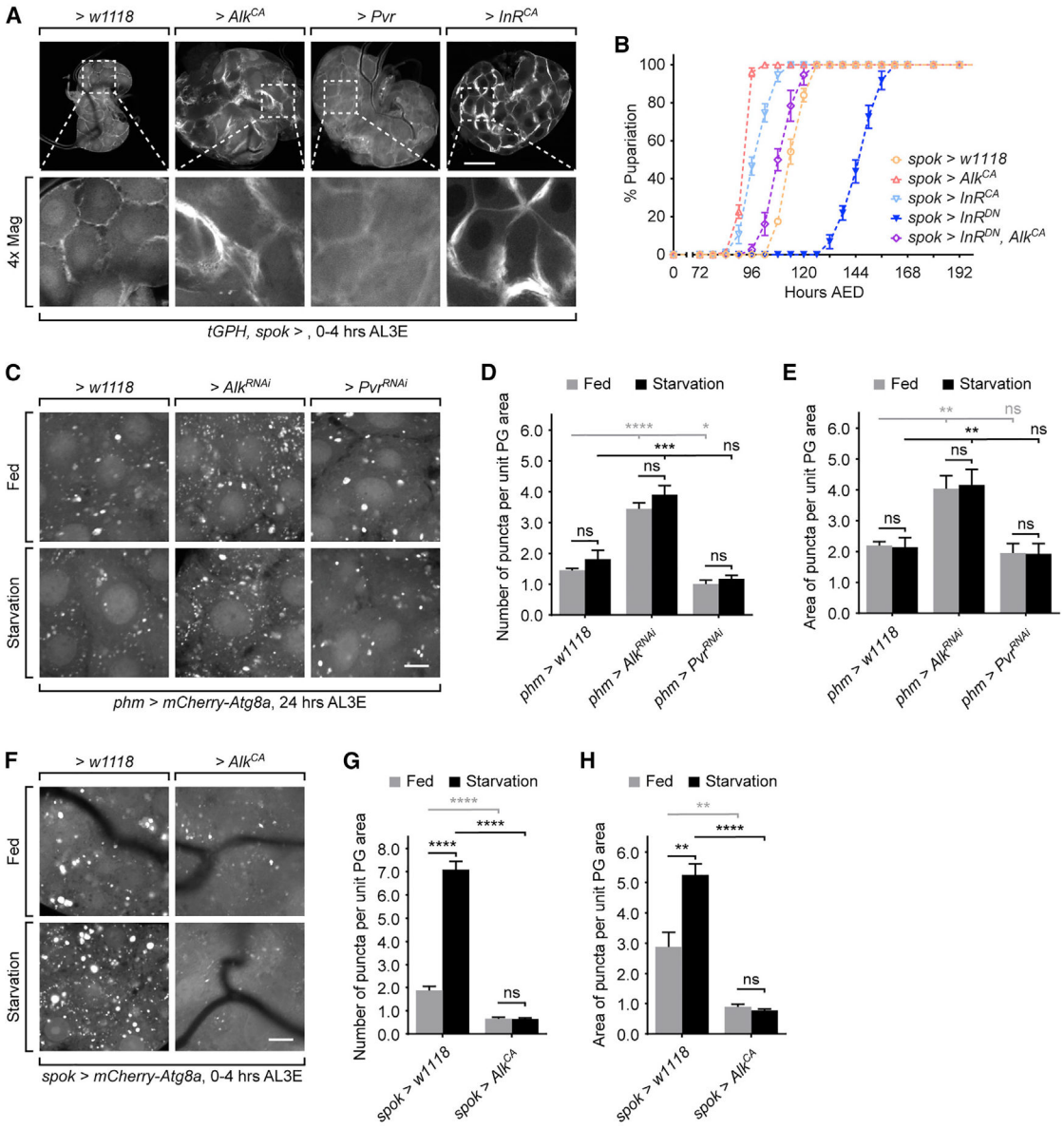

Figure 3. Alk regulates autophagy in the PG by activating the PI3K/Akt pathway

(A) Images of *spok>w1118*, *spok>Alk^CA^*, *spok>Pvr*, and *spok>InR^CA^* PGs expressing tGPH. Enlarged images of indicated areas are also shown. Scale bar, 50 μm.

(B) Pupariation timing curves of *spok>w1118*, *spok>Alk^CA^*, *spok>InR^CA^*, *spok>InR^DN^*, and *spok>InR^DN^*,*Alk^CA^* larvae.

(C) Images of *phm>w1118*, *phm>Alk^RNAi^*, and *phm>Pvr^RNAi^* PGs expressing mCherry-Atg8a. Animals were starved at 24 h AL3E for 4 h to induce autophagy. Scale bar, 10 μm.

(D and E) Quantification of the number (D) and the total area (E) of Atg8a-positive puncta per unit of PG cell area.

(F) Images of *spok>w1118* and *spok>Alk^CA^* PGs expressing mCherry-Atg8a. Animals were starved at 0–4 h AL3E for 4 h to induce autophagy. Scale bar, 10 μm.

(G and H) The number (G) and total area (H) of Atg8a-positive puncta per unit of PG cell area.

(D–G and H) Mean ± SEM; p values by unpaired t test (n = 5–7; *p < 0.05, **p < 0.01, ***p < 0.001, ****p < 0.0001).

See also Figure S2.

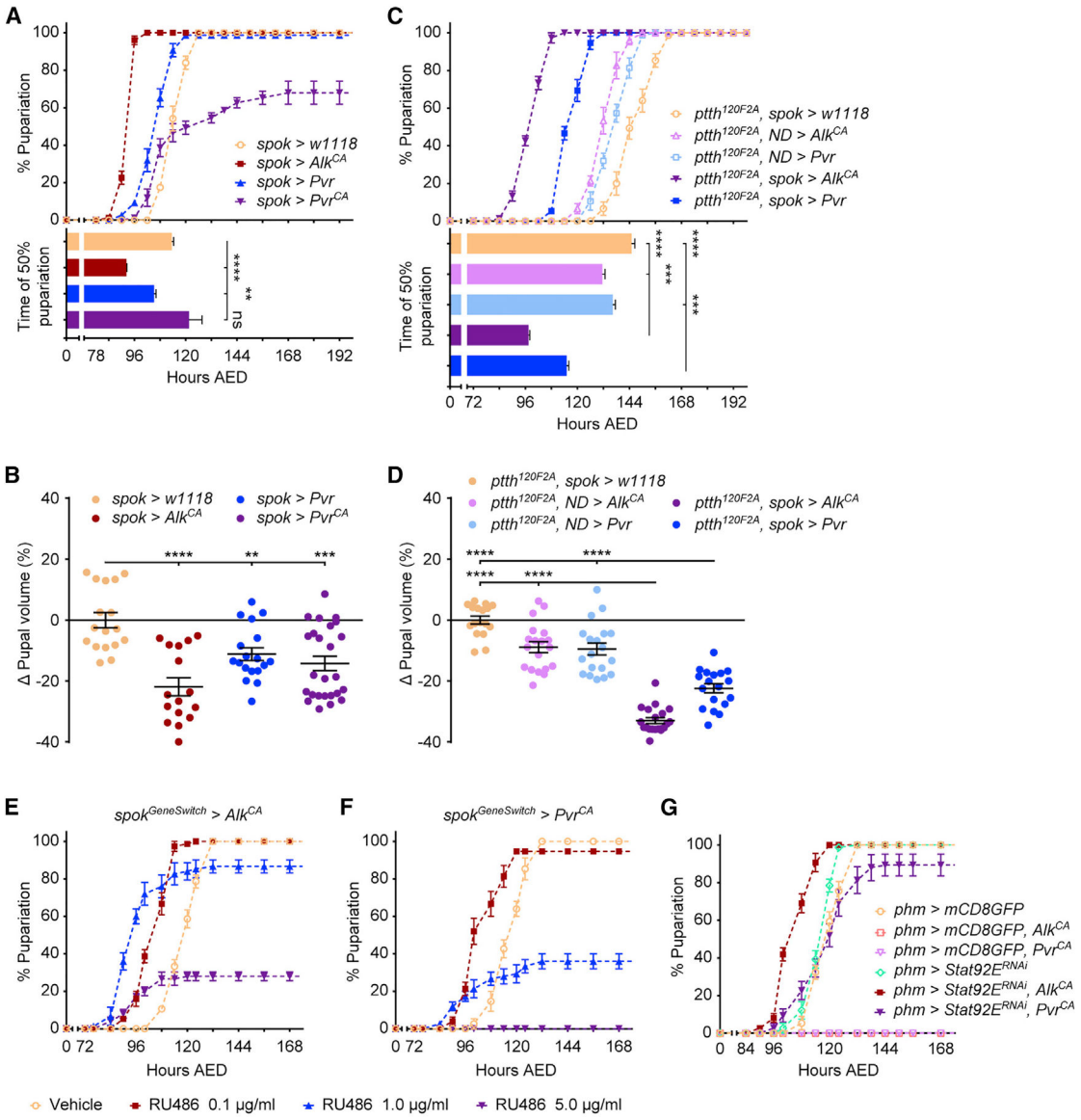

Figure 4. Activation of Alk and Pvr pathway affects developmental timing in a dose-dependent manner

(A) Pupariation timing curves and the time of 50% pupariation of *spok>w1118*, *spok>Alk^CA^*, *spok>Pvr*, and *spok>Pvr^CA^* larvae.

(B) Relevant pupal volume changes in animals tested in (A).

(C) Pupariation timing curves and the time of 50% pupariation of *spok>w1118*, *spok>Alk^CA^*, and *spok>Pvr* larvae with *ptth^120F2A^* mutant background.

(D) Relevant pupal volume changes in animals tested in (C).

(E and F) Pupariation timing curves of *spok^GeneSwitch^>Alk^CA^* (E) and *spok^GeneSwitch^>Pvr^CA^* (F) larvae fed with indicated concentrations of RU486.

(G) Pupariation timing curves of *phm>w1118*, *phm>Alk^CA^*, and *phm>Pvr^CA^* larvae with/without knockdown of *Stat92E*. To balance the strength of *phm-Gal4* driver, a *UAS-mCD8GFP* transgene was introduced to the groups without *UAS-Stat92E^RNAi^*.

(A–D) Mean ± SEM; p values by unpaired t test (n = 3 in A and C, n = 16–25 in B and D; **p < 0.01, ***p < 0.001, ****p < 0.0001).

See also Figure S3.

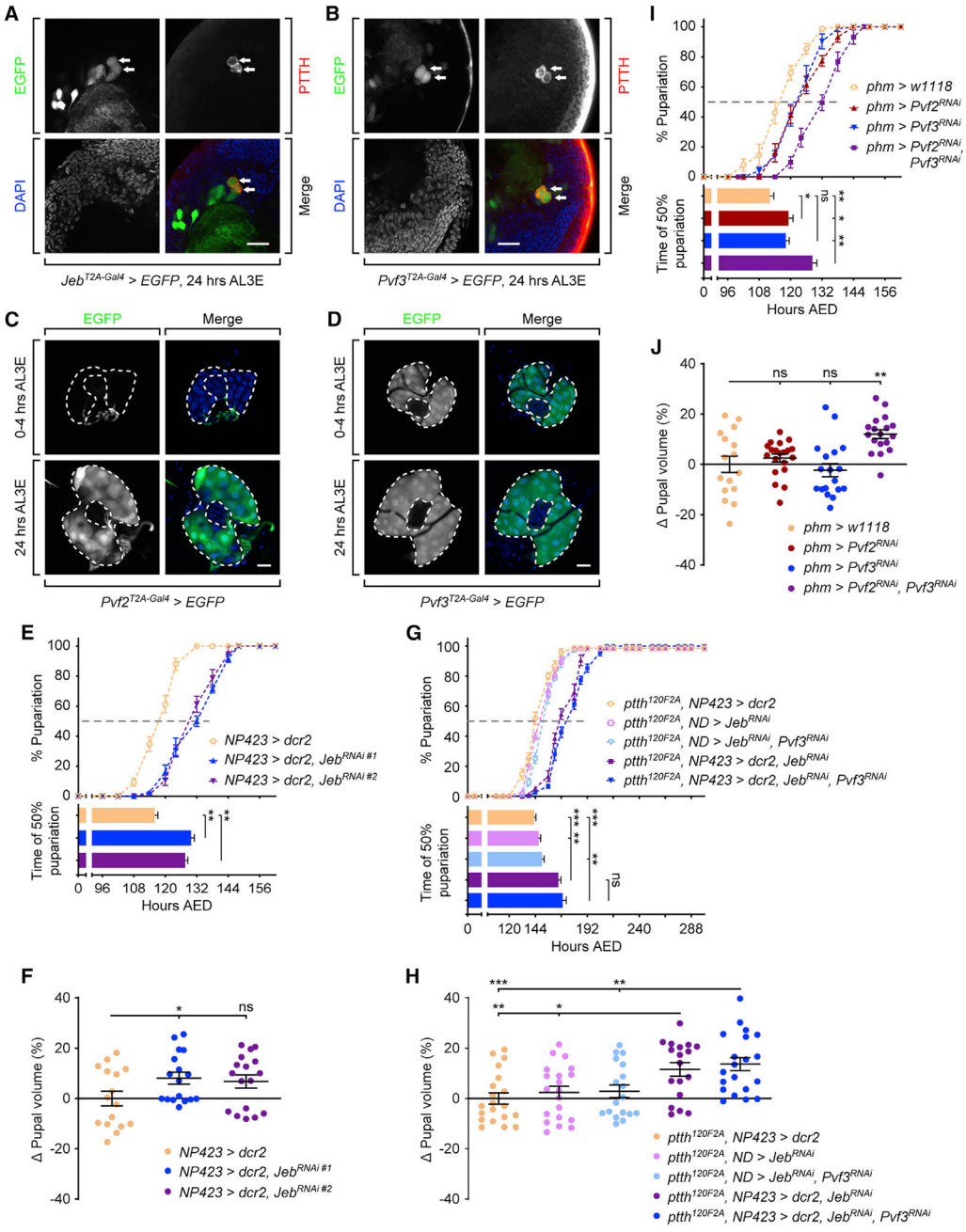

Figure 5. Ligands that activate Alk and Pvr derive from both PGNs and PG

(A and B) Immunofluorescence images of *jeb*$^{T2A\text{-}Gal4}$>*EGFP* (A) and *Pvf3*$^{T2A\text{-}Gal4}$>*EGFP* (B) larval brains stained with anti-PTTH antibody. Arrows indicate the colocalization between the EGFP and PTTH immunofluorescence signals. Scale bars, 20 μm.

(C and D) Images of *Pvf2*$^{T2A\text{-}Gal4}$>*EGFP* (A) and *Pvf3*$^{T2A\text{-}Gal4}$>*EGFP* (B) PGs that have expression of EGFP in Pvf2- and Pvf3-expressing cells. Dash line marks the outline of PG area in the ring gland. Scale bars, 50 μm.

(E) Pupariation timing curves and the time of 50% pupariation of *NP423>w1118* and two groups of *NP423>jeb*^{RNAi} larvae.

(F) Relevant pupal volume changes in animals tested in (E).

(G) Pupariation timing curves and the time of 50% pupariation of *NP423>jeb^{RNAi}* and *NP423>jeb^{RNAi},Pvf3^{RNAi}* larvae with *ptth^{120F2A}* mutant background.

(H) Relevant pupal volume changes in animals tested in (G).

(I) Pupariation timing curves and the time of 50% pupariation of *phm>w1118*, *phm>Pvf2^{RNAi}*, *phm>Pvf3^{RNAi}* and *phm>Pvf2^{RNAi},Pvf3^{RNAi}* larvae.

(J) Relevant pupal volume changes in animals tested in (I).

(E–J) Mean ± SEM; p values by unpaired t test (n = 3 in E and I, n = 16–20 in F and J; *p < 0.05, **p < 0.01).

See also Figure S4.

KEY RESOURCES TABLE

REAGENT or RESOURCE	SOURCE	IDENTIFIER
Antibodies		
Alk	Gift from Dr. Ruth Palmer, University of Gothenburg, Sweden	N/A
Pvr	Gift from Dr. Ben-Zion Shilo, Weizmann Institute, Israel	N/A
phospho-Erk	Sigma Aldrich	Cat#M8159
Chemicals, peptides, and recombinant proteins		
RU486 (Mifepristone)	Sigma Aldrich	Cat#M8046
Paraformaldehyde, 16% Aqueous Solution	Electron Microscopy Sciences	Cat#15700
TRIzol Reagent	Invitrogen	Cat#15596026
SuperScript III Reverse Transcriptase	Invitrogen	Cat#18080093
Critical commercial assays		
20-Hydroxyecdysone EIA Kit	Cayman Chemical	Cat#501390
FISH Tag RNA Multicolor Kit	Invitrogen	Cat#F32956
RNeasy Mini Kit	QIAGEN	Cat#74104
Experimental models: Organisms/strains		
Drosophila Pvf1 ^{EP1624}	BDSC	RRID: BDSC_11450
Drosophila Pvf2^{T2A}*-Gal4*	This manuscript	N/A
Drosophila Pvf3^{T2A}*-Gal4*	This manuscript	N/A
Drosophila jeb^{T2A}*-Gal4*	This manuscript	N/A
Drosophila ptth ^{120F2A}	Shimell et al., 2018	N/A
Drosophila phm-Gal4	Ono et al., 2006	RRID: BDSC_80577
Drosophila spok-Gal4	Moeller et al., 2017	N/A
Drosophila spok^{GeneSwitch}*-Gal4*	Zeng et al., 2020	N/A
Drosophila NP423-Gal4	Yamanaka et al., 2013b	N/A
Drosophila Dome-Gal4	Ghiglione et al., 2002	N/A
Drosophila UAS-Alk ^{CA}	Zettervall et al., 2004	N/A
Drosophila UAS-Alk ^{DN}	Bazigou et al., 2007	N/A
Drosophila UAS-jeb	Varshney and Palmer, 2006	N/A
Drosophila UAS-Pvr	BDSC	RRID: BDSC_58998
Drosophila UAS-Pvr ^{CA}	BDSC	RRID: BDSC_58428
Drosophila UAS-Pvr ^{DN}	BDSC	RRID: BDSC_58431
Drosophila UAS-Pvf2	Gift from Dr. Edan Foley, University of Alberta, Canada	N/A
Drosophila UAS-Pvf3	Gift from Dr. Edan Foley, University of Alberta, Canada	N/A
Drosophila UAS-InR ^{CA}	BDSC	RRID: BDSC_8440
Drosophila tGPH	BDSC	RRID: BDSC_8163
Drosophila 10xStat92E-GFP	BDSC	RRID: BDSC_26197
Drosophila UAS-Alk ^{RNAi}	BDSC	RRID: BDSC_27518

REAGENT or RESOURCE	SOURCE	IDENTIFIER
Drosophila UAS-btl ^{RNAi}	BDSC	RRID: BDSC_40871
Drosophila UAS-Cad96Ca ^{RNAi}	BDSC	RRID: BDSC_55877
Drosophila UAS-CG10702 ^{RNAi}	BDSC	RRID: BDSC_42663
Drosophila UAS-Ddr ^{RNAi}	BDSC	RRID: BDSC_55906
Drosophila UAS-dnt ^{RNAi}	BDSC	RRID: BDSC_67251
Drosophila UAS-drl ^{RNAi}	BDSC	RRID: BDSC_39002
Drosophila UAS-Drl-2 ^{RNAi}	BDSC	RRID: BDSC_55893
Drosophila UAS-Egfr ^{RNAi}	BDSC	RRID: BDSC_25781
Drosophila UAS-Eph ^{RNAi}	BDSC	RRID: BDSC_39066
Drosophila UAS-ht ^{RNAi}	BDSC	RRID: BDSC_35024
Drosophila UAS-InR ^{RNAi}	BDSC	RRID: BDSC_51518
Drosophila UAS-Nrk ^{RNAi}	BDSC	RRID: BDSC_55184
Drosophila UAS-otk ^{RNAi}	BDSC	RRID: BDSC_55869
Drosophila UAS-Pvr ^{RNAi}	BDSC	RRID: BDSC_37520
Drosophila UAS-Ret ^{RNAi}	BDSC	RRID: BDSC_55872
Drosophila UAS-Ror ^{RNAi}	BDSC	RRID: BDSC_62868
Drosophila UAS-sev ^{RNAi}	BDSC	RRID: BDSC_55866
Drosophila UAS-Tie ^{RNAi}	BDSC	RRID: BDSC_54005
Drosophila UAS-tor ^{RNAi}	BDSC	RRID: BDSC_33627
Drosophila UAS-Stat92E ^{RNAi}	BDSC	RRID: BDSC_33637
Drosophila UAS-jeb ^{RNAi}	BDSC	RRID: BDSC_56022
Drosophila UAS-Pvf2 ^{RNAi}	BDSC	RRID: BDSC_61955
Drosophila UAS-Pvf3 ^{RNAi}	BDSC	RRID: BDSC_38962
Drosophila UAS-Alk ^{RNAi}	VDRC	Stock #107083; RRID: FlyBase_FBst0478906
Drosophila UAS-Pvr ^{RNAi}	VDRC	Stock #43459; RRID: FlyBase_FBst0465099
Drosophila UAS-Pvr ^{RNAi}	VDRC	Stock #43461; RRID: FlyBase_FBst0465100
Drosophila UAS-Pvr ^{RNAi}	VDRC	Stock #105353; RRID: FlyBase_FBst0477180
Drosophila UAS-jeb ^{RNAi}	VDRC	Stock #103047; RRID: FlyBase_FBst0474909
Drosophila UAS-Pvf2 ^{RNAi}	VDRC	Stock #7629; RRID: FlyBase_FBst0470770
Drosophila UAS-Pvf3 ^{RNAi}	VDRC	Stock #37933; RRID: FlyBase_FBst0462241
Drosophila UAS-Pvf2 ^{RNAi}	NIG	Stock #13780R-2
Drosophila UAS-Pvf3 ^{RNAi}	NIG	Stock #13781R-1
Software and algorithms		
ImageJ	ImageJ-NIH	https://imagej.nih.gov/ij/index.html
GraphPad Prism	GraphPad Software	https://www.graphpad.com/scientific-software/prism/